Accepted Manuscript

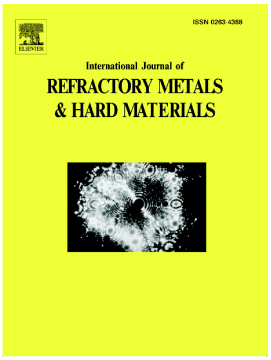

Micromechanical and microstructural properties of tungsten fibers in the as-produced and annealed state: Assessment of the potassium doping effect

D. Terentyev, L. Tanure, A. Bakaeva, A. Dubinko, V. Nikolić, J. Riesch, K. Verbeken, S. Lebediev, E.E. Zhurkin

PII: S0263-4368(19)30101-5
DOI: https://doi.org/10.1016/j.ijrmhm.2019.03.012
Reference: RMHM 4916

To appear in: *International Journal of Refractory Metals and Hard Materials*

Received date: 8 February 2019
Revised date: 5 March 2019
Accepted date: 10 March 2019

Please cite this article as: D. Terentyev, L. Tanure, A. Bakaeva, et al., Micromechanical and microstructural properties of tungsten fibers in the as-produced and annealed state: Assessment of the potassium doping effect, International Journal of Refractory Metals and Hard Materials, https://doi.org/10.1016/j.ijrmhm.2019.03.012

This is a PDF file of an unedited manuscript that has been accepted for publication. As a service to our customers we are providing this early version of the manuscript. The manuscript will undergo copyediting, typesetting, and review of the resulting proof before it is published in its final form. Please note that during the production process errors may be discovered which could affect the content, and all legal disclaimers that apply to the journal pertain.

ACCEPTED MANUSCRIPT

Micromechanical and microstructural properties of tungsten fibers in the as-produced and annealed state: assessment of the potassium doping effect

D. Terentyev[1], L. Tanure[2,3], A. Bakaeva[1], A. Dubinko[1], V. Nikolić[4], J. Riesch[5], K. Verbeken[2], S.Lebediev[6], E.E. Zhurkin[7]

[1]*Structural Materials Group, Institute of Nuclear Materials Science, SCK·CEN, Mol, 2400, Belgium*

[2]*Department of Materials, Textiles and Chemical Engineering, Ghent University (UGent), Technologiepark 903, B-9052 Ghent, Belgium*

[3]*Dutch Institute for Fundamental Energy Research, DIFFER, De Zaale 20, 5612 AJ Eindhoven, The Netherlands*

[4]*Erich Schmid Institute of Materials Science of the Austrian Academy of Sciences, Leoben, Austria*

[5]*Max-Planck-Institut für Plasmaphysik, 85748 Garching, Germany*

[6]*V.N. Karazin Kharkiv National University, 4 Svobody Sq., Kharkiv, 61022, Ukraine*

[7]*Peter the Great St. Petersburg Polytechnic University (SPbPU), Russia, 195251, St. Petersburg, Polytechnicheskaya, 29*

Abstract

Due to its high strength and low temperature ductility, tungsten fibers (W_f) have been widely used as reinforcement elements in metallic, ceramic and glass matrix composites to improve the strength, toughness and creep resistance. Materials designed for future fusion reactors also utilize the option of W_f reinforcement, i.a. with a copper (W_f/Cu) or tungsten (W_f/W) matrix. W_f/W composites are being intensively studied as risk-mitigation materials to replace bulk tungsten which is susceptible to embrittlement induced by neutrons resulting from fusion reaction. Operation of W_f/W in high temperatures (up to 1300°C and even higher) fusion environment implies a risk of recrystallization and grain growth, which dimishes the attractive properties of tungsten fibers. In this work, we assess this modification of micro-mechanical and microstructural properties of tungsten fibers by means of nanoindentation, scanning electron microscopy, electron back-scattering diffraction analysis and corelate it with the ultimate tensile strength and fracture modes observed in the tensile tests. Both pure W and pottasium doped wires in the as-fabricated and annealed states are investigated and the results are compared with bulk tungsten, also exposed to several annealing temperatures. The results highlight the postive impact of potassium doping which shifts the threshold temperature for the grain growth by about 600°C compared to pure tungsten wire. The results of the nanoindentation revealed systematic linear correlation with the ultimate tensile strength, which therefore offers a complimenatary way of micro-mechanical testing linking it with macro-scale properties of the wires.

Keywords: Tungsten, fiber, plasticity, recrystallization, potassium doped, annealing, composites.

corresponding author: dterenty@sckcen.be

ACCEPTED MANUSCRIPT

1. Introduction

Development of materials for future applications requires new approaches, advanced technology for massive-scale fabrication and fine-scale tuning of the products. When it comes to the materials with structural applications, extending the operational/environmental range while sustaining toughness and strength is a typical challenge in the design materials from nuclear [1] to biomedical applications [2]. One of the options, widely used to improve the overall properties of metallic [3, 4], glass [5] and ceramic materials [6, 7], is the so-called fiber-reinforced composite component, which consists of (i) fiber – being a discontinuous inclusion; (ii) matrix, being a continuous phase or media and (iii) interface, e.g. a coating of the fiber ensuring its proper operation being embedded in the matrix. The properties of fibers, being reinforcement elements, are therefore critical with respect to the performance and operational fatigue of the composites. In that respect, the usage of tungsten fibers (W_f) to strengthen metallic materials has been intensively explored over the last decade as an option to improve tungsten materials for fusion applications in the "in-vessel" region (i.e. the region in direct contact with plasma and/or harsh irradiation media resulting from D + T = He + neutron fusion reaction) [8-10].

The recent progress in the research dedicated to the plasma-facing materials resulted in the re-assessment of the first wall material for divertor components in ITER and DEMO, for which tungsten was selected in favour to carbon-based composite [9]. However, one of the most critical issues still to be addressed by material science and engineering communities is the embrittlement induced by 14 MeV neutrons [11, 12], which severely impacts the fracture toughness of bulk tungsten metal. The cyclic heat loads will contribute to the recrystallization and grain growth [13] also causing loss of toughness. Hence, the development of W_f-W composite is considered as one of the options to mitigate the operational embrittlement [9].

In fact, the drawn tungsten wire was already commercially applied more than 100 years ago in the illumination industry as the main filament element for street lighting [14]. The problem of creep and thermal fatigue (light on - light off) lead to the discovery of potassium (K) doping as solution to the problem [15, 16]. Later on, it was recognized that K-doping suppresses recrystallization and grain growth by forming precipitates at grain boundaries, thereby preventing their thermal diffusion and coarsening [17]. More recent research was therefore focused on the understanding of the extension of the positive impact of K-doping with respect to the thermal stability of the microstructure at very high temperatures (required for the sintering of the composites or expected in the fusion environment due to plasma instabilities), as well as the evolution of mechanical properties of the annealed wires.

The tensile mechanical properties of pure W and K-doped wires were studied at room and elevated temperatures by groups of Riesch [18-21] and Terentyev [22-25]. The primary conclusion regarding the potassium doping that can be drawn from those studies is that it helps suppressing massive grain growth at least up to 1600°C for 30 min, remaining ductile at room temperature with ultimate tensile strength exceeding 1 GPa. Annealing above 1900°C causes strong reduction of the tensile strength at elevated temperature (down to ~0.1 GPa at 500°C) and makes the wire fully brittle at room temperature.

Jansen conducted the annealing experiments to investigate the aspects of recrystallization kinetics of doped and undoped tungsten wires [26]. Small uniform microstructural changes of the grains changing from "ribbon-shaped" fiber crystals to "stem-like" crystals were observed and ascribed to the recrystallization phenomenon in un-doped wire during the annealing at 1600°C. In the case of

ACCEPTED MANUSCRIPT

doped W wires, the recrystallization fraction was seen to reach 100% upon annealing temperature (for ~ 1 hour duration) exceeding 2200°C. Primary recrystallization was characterized by small morphological changes in the grains. Jansen concluded that the temperature needed to start the exaggerated grain growth is above 2000°C. Such a high temperature limit was explained by the effective dragging of grain boundary migration by the dopant remnants.

In a recent study carried out by Zhao et al.[20], pure tungsten wires produced by the same route were annealed at 1000°C for 3h and at 1627°C for 30min. After annealing at 1627°C grains became equiaxed and limited microstructural coarsening was reported, which also ascribed to the recrystallization. Furthermore, Nikolić et al. performed microstructural characterization of both pure and potassium doped tungsten wires, annealed for 1h in the temperature range from 900 to 1600°C [27]. The full recrystallization was observed above 1300°C for the undoped material, while the potassium doped wires showed only milder microstructural changes, consequently suppressing recrystallization and grain growth to temperatures above 1600°C.

Potassium is introduced via KSiAl-doping particles, which decompose during sintering of the ingots and most of Si and Al elements are remove [28]. Since potassium is insoluble in tungsten it clusterizes inside the residual pores and crystallographic defects (grain boundaries) of the tungsten ingots. During the extrusion of the wires from the sintered ingots, the potassium clusters become elongated in the drawing direction forming small ellipsoids located at the grain boundary interfaces. Under annealing, these potassium clusters start to diffuse and coalesce into a single row of nanometric bubbles which further suppress thermally-driven diffusion and grain boundaries. Up to now, the detailed comparative microstructural investigation characterizing grain structure of pure and K-doped tungsten under progressive increase of the annealing temperature from 1300°C and above 2000°C (i.e threshold temperature according to Jansens [26]) is still missing.

In this work, we have performed a combined experimental investigation of the impact of high temperature annealing on the micro-mechanical and microstructural properties of tungsten wires. Particular focus was put on the understanding of the role played by potassium doping in the recrystallization process occurring under annealing made in several steps to reach 2100°C. Firstly, we summarize the results of tensile tests of the as-fabricated and annealed wires performed in previous studies [22, 24]. Then we proceed with a systematic analysis of the fracture surface of the samples tested at room and elevated temperature, microstructural characterization of grain morphology by electron backscattering diffraction analysis, and nanoindentation testing. The obtained results are also compared with the data collected for the bulk forged tungsten subject to the high temperature annealing.

The obtained results are summarized and discussed in the light of the relevance of sub-miniaturized mechanical testing (like nanoindentation) to predict the strength otherwise measured in the conventional tensile tests. As will be shown, a good linear correlation between the ultimate tensile strength (UTS) and nanoindentation hardness is found for both pure and K-doped tungsten wires as long as the mechanical response is controlled by fine µm-sized grain microstructure (i.e. prior the massive recrystallization). The observation opens a perspective to use nanoindentation testing for further characterization of the impact of irradiation or fatigue damage on the strength of tungsten wires for W_f/W composites.

2. Materials and experimental procedures

2.1 Tungsten wires and bulk tungsten

ACCEPTED MANUSCRIPT

Drawn potassium doped (60–75 ppm) and pure tungsten wires, identical to the wires used in [22, 23, 29] were provided by the OSRAM GmbH, Schwabmünchen. The diameter of the wires was measured to be 148.7 ± 0.2 µm [29]. Measurements were performed by high resolution optical microscopy. Basic information of the grain microstructure of the wires in the as-received condition has been reported in [20, 22, 23, 29]. The grains are strongly elongated in the direction of wire axis and form curled structure in the wire cross-section. The size of grains in the wire's cross-section varies from 0.1 up to 1 µm. In the longitudinal cross-section, the interior of grains was reported to contain high density of dislocation defects and dislocation boundaries [20]. The grain size along the wire axis was estimated to be in the range 10-40 µm. The K-doped and pure W wires were cut into pieces of 100 mm and these were annealed at 1000°C, 1300°C, 1600°C, 1900°C, and 2100°C. The highest and lowest annealing temperature was not used for pure and doped W wire respectively. For the doped W wire, the changes in the microstructure after annealing at 1000°C were considered to be minor, based on the previously performed experiments. While, in the case of pure W wire, the experience has shown that the annealing at 1900°C already makes the wire completely brittle at room temperature, thus offering no technological interest of studying higher annealing temperatures. The straightened and cut wire pieces were then annealed in a tube furnace under hydrogen atmosphere at Osram GmbH. During this process the samples were placed on a shovel (carbon free) and kept at mentioned temperatures for 30 min.

In addition to W wires, bulk tungsten samples in stress-relieved and annealed conditions were also investigated. Polycrystalline W with purity of 99.97%, provided by Plansee AG as a bar with a square cross-section of 36 mm, was used in this study and in our previous works. Details about impurities and microstructure can be found in [30, 31]. This material was fabricated by hammering on both sides. After production, the block was stress-relieved at 1273 K for one hour in an inert environment. Electron back scatter diffraction (EBSD) analysis revealed that the microstructure of this material consisted of randomly textured elongated grains, containing multiple low angle grain boundaries within the elongated structure and separated mainly by high-angle grain boundaries. Grains with high misorientation angle are randomly oriented and are elongated with a size of 5-20 µm and 10-100 µm, normal and along to the bar axis, respectively. The presence and morphology of sub-grains was studied by transmission electron microscopy in [30], which revealed sub-grains (also elongated) with size varied in the range 0.6 – 1.7 µm and 2.3 – 4 µm, respectively, normal to and along the elongation directions. The dislocation density is found to be (4-8)×10^{12} m^{-2}, depending on particular sub-grain and is being 4.5×10^{12} m^{-2} on average. Similar microstructural characterization was performed for this material annealed at 1300°C, 1500°C and 1800°C in exactly the same conditions (i.e. furnace, atmosphere, time) as above discussed wires, and the results of EBSD and TEM analysis are published in [32]. In the following, we shall compare the response of bulk W and W wires to the indentation given the similarity of the annealing conditions (i.e. the same annealing method and temperature range was investigated).

2.2 EBSD measurements

EBSD measurements were performed on the longitudinal sections which were cut from the wires broken in the uni-axial tensile tests. The pieces were cut from the parts taken at a distance of ~10 mm from the neck. Pieces of 10 mm length were prepared following the standard metalographic procedures of cutting, mounting, grinding and polishing. The EBSD analysis were carried out using a Field Emission Gun Quanta-450 FEI Scanning Electron Microscope with 20kV acceleration voltage. Here, we focus our analysis on the longitudinal cross-sections since this allows us to understand the evolution of the microstructure of elongated grains, which is of crucial importance for the low temperature ductility of the wires. The analyzed areas varied from 50 x 100 μm^2 to 150 x 900 μm^2,

ACCEPTED MANUSCRIPT

depending on the specific annealing conditions and the wire type. The step-sizes ranged from 50 to 400nm depending on the scanned area. During the image post-processing with OIM® Analysis software, the Neighbor Confidence Index (CI) Correlation and the Grain CI Standardzation data cleanup were applied, followed by removal of points with Confidence Index lower than 0.1. To evaluate both length and width of the grains, the linear intercept method was used in the horizontal and vertical directions, respectively.

2.3 Nanoindentation measurements

After the EBSD measurements, the samples were submitted for the nanoindentation testing. Nanoindentation testing was performed with an Agilent G200 nanoindenter using Continuous Stiffness Mode (CSM) [33] in order to determine the Young's modulus and hardness. The standard XP head equipped with a Berkovich diamond tip was used. The oscillation amplitude and frequency were 2 nm and 45 Hz respectively, the indentation strain rate – 0.05 s^{-1} and the penetration depth *h* – 1.5 µm. At least 16 indents per sample ,spaced by 40 µm, were performed and hardness was estimated using the classical Oliver & Pharr method [33]. Indents were done in the central part of the wire (as close as technically possible to target) in one row. To provide information on the exact position of the indentation, the tested samples were inspected by scanning electron microscopy (SEM, JEOL JSM-6610LV), using a secondary electron (SE) detector and operating conditions were: 20 kV accelerating voltage and 10-15 mm working distance.

3. Results

3.1 Overview of the mechanical properties obtained from tensile tests

The most important and most-reliably determined mechanical property of the wire in the view of the reinforcement application is its ultimate tensile strength, while the reduction of the cross-section area is another important feature reflecting the amount local (i.e. in the necking region) plastic deformation [34]. Indeed, as earlier studies show the determination of the true strain of the whole sample is complicated due to the formation of multiple necking regions [24], while determination of the yield stress is somewhat unambigous because the fabrication of standardized samples from 150 µm wire is impossible. Correspondingly, here we report the ultimate tensilie strength (UTS) which was measured at 22°C (RT), 300°C and 500°C for the two sets of wires annealed in the temperature range 1000-2300°C. The detailed description of the study of mechanical properties is reported in [24]. The UTS and important features of the fracture surface are summarized in Figs. 1, 2 and 3, respectively, for T_{test}=22 (RT), 300°C and 500°C.

The results of tests performed at RT are summarized in Fig.1. We can see that for pure W wire, the annealing at 1600°C and above makes the wire completely brittle, such that the fracture occurs in the elastic region without any yield. However, even moderate annealing at 1000°C and 1300°C causes progressive nearly-linear reduction of the ultimate tensile strength down to 1 GPa, compared to ~2.5 GPa in the as-fabricated state. The same strong reduction of UTS is seen at T_{test}=300°C and 500°C, see Figs. 2 and 3. In the case of K-doped wires tested at RT, UTS does not drop below 1.5 GPa up to the annealing temperature of 1600°C, followed by less steep decrease down to 1 GPa after annealing at 2100°C. The trends registered for the wire strength in the tests performed at 300°C and 500°C are very similar. Namely, there is a linear decrease up to 1900°C followed by a steeper decrease at 2100°C. For T_a=2300°C, no further change in the strength is detected.

ACCEPTED MANUSCRIPT

Fig.1(a) shows a typical pattern of the fracture surface being delaminated fine-scale grains or so-called knife-edge grains [29, 35]. Contrary to that, Fig.1(b) shows the fracture surface of the pure W wire annealed at 1300°C , where typical mixture of trans- and inter-granular fracture can be seen, but no delamination. After annealing at 1600°C, see Fig.1(c), intergranular fracture appears to be the dominant mode, as patters of grains are clearly seen. In the case of K-doped wire, the reduction of UTS down to ~1 GPa is observed after annealing at 2100°C and this is where the fracture occurs by cleavage as is shown in Fig.1(d).

Tests performed at elevated temperature show the same trends as observed at RT, except that the plastic deformation of pure W wire is now registered at all annealing temperatures. Noticeably, UTS of pure W wire drops below 250 MPa (i.e. factor 10 compared to the UTS in the fabricated state) after annealing at 1600°C and above. The fracture surface shown in Fig.2(a), which corresponds to the neck-to-edge deformation i.e. 100% reduction of the fracture area, implies that the wire strength is controlled by the dislocation slip in this region. Contrary to that, in the K-doped wires the fracture surface has features of cleavage and crack deflection (steps on the fracture surface), see Fig.2(b). No longitudinal cracks, which are often observed on the surface of the as-fabricated wire (with and without K-doping), are seen in this case.

However, in some cases, the cleavage was observed in pure W despite very high recrystallization temperature and test temperature, where we would expect to see neck-to-edge. An example of such pattern is shown in Fig.3(a) for the wire tested at 500°C after annealing at 1900°C . The investigation of the microstructure along the wire revealed that the necking region was formed just near the fracture point. Hence, we interpret this as the location of the grain boundary which retained after annealing and caused the stress-localization under deformation. As a result of continuous deformation, the critical stress intensity near grain boundary was reached sooner than the complete necking. Typical cleavage and deflection of the crack moving across the grain boundary can be seen in Fig.3(a).

UTS of K-doped wires annealed at 2100°C also strongly goes down and becomes comparable to the one of pure W annealed at 1900°C, as can be seen from Fig. 2 and 3. However, the fracture surface reveals some difference, which was especially pronounced in tests at 500°C. Consider the fracture surface patterns shown in Fig.3 (a) and (b). While in pure W wire, the fracture surface is nearly flat, the K-doped wire exhibits necking region and flat surface in the central part of the wire. Fine details of the fracture surface in the central region point to the occurrence of the transgranular fracture mode, but the size of the grains is about few μm. This observation suggests that the recrystallization in the K-doped wires was not completed in the central part of the wire even at 2100°C, which could explain why the wire retains rather high strength at room temperature. To clarify this point, we move to the presentation of the results of EBSD measurements which will unambiguously reveal the pattern of grains depending on the annealing temperature.

ACCEPTED MANUSCRIPT

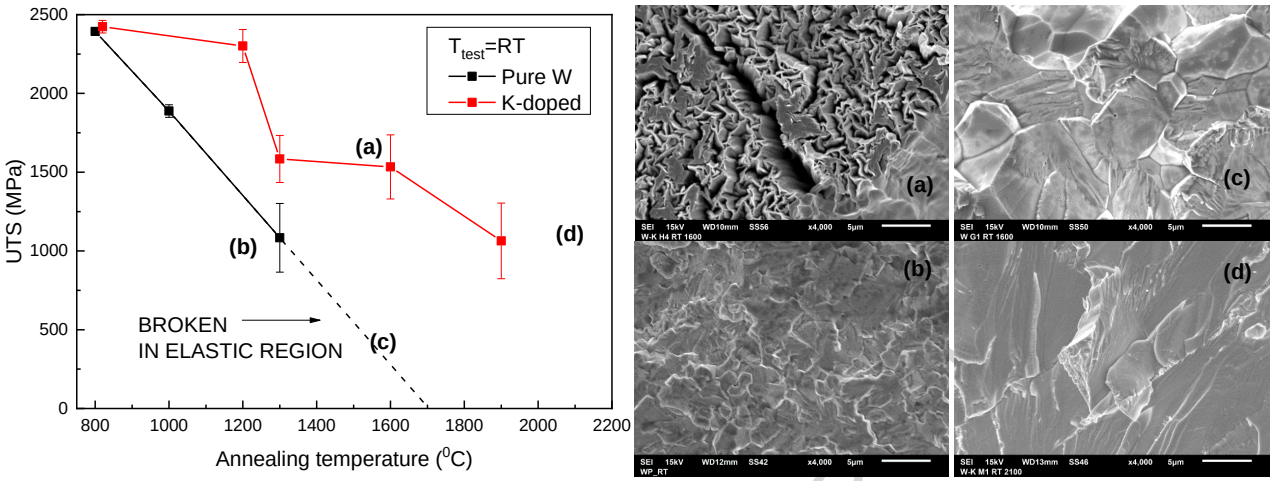

Fig.1 Ultimate tensile strength vs annealing temperature for wires tested at RT. Insets on the right show the fracture surface of (a) K-doped wire annealed at 1600°C; (b) pure W wire annealed at 1300°C; (c) pure W wire annealed at 1600°C; (d) K-doped wire annealed at 2100°C. Results presented at T_a=800°C correspond to the as-fabricated state.

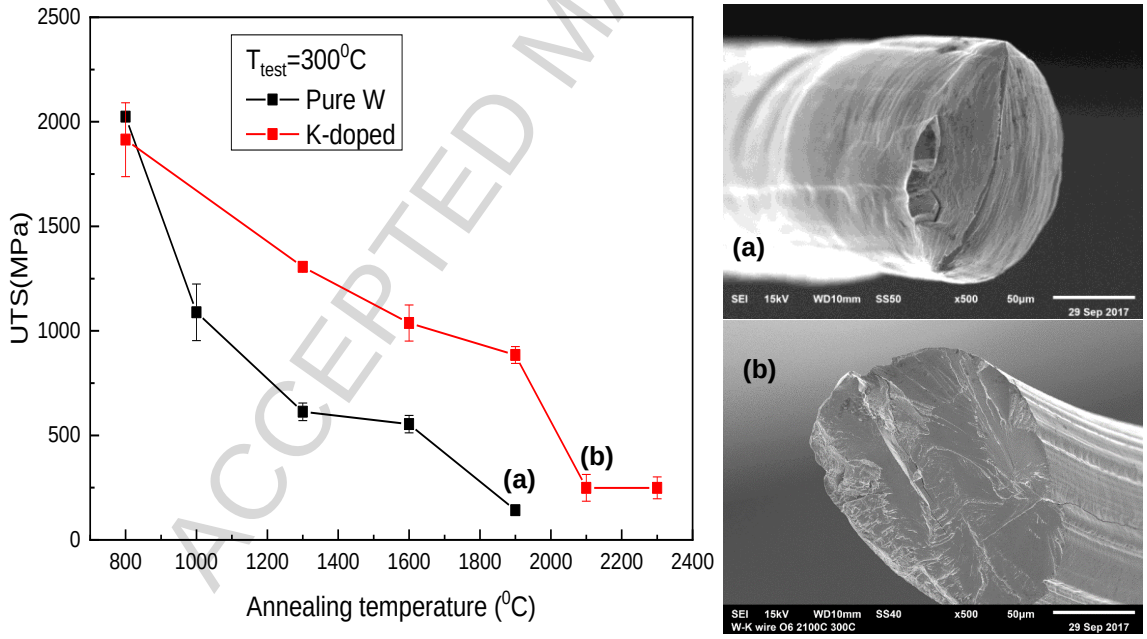

Fig.2. Ultimate tensile strength vs annealing temperature for wires tested at 300°C. Insets on the right show the fracture surface of (a) pure W wire annealed at 1900°C and (b) K-doped wire annealed at 2100°C. Results presented at T_a=800°C correspond to the as-fabricated state.

ACCEPTED MANUSCRIPT

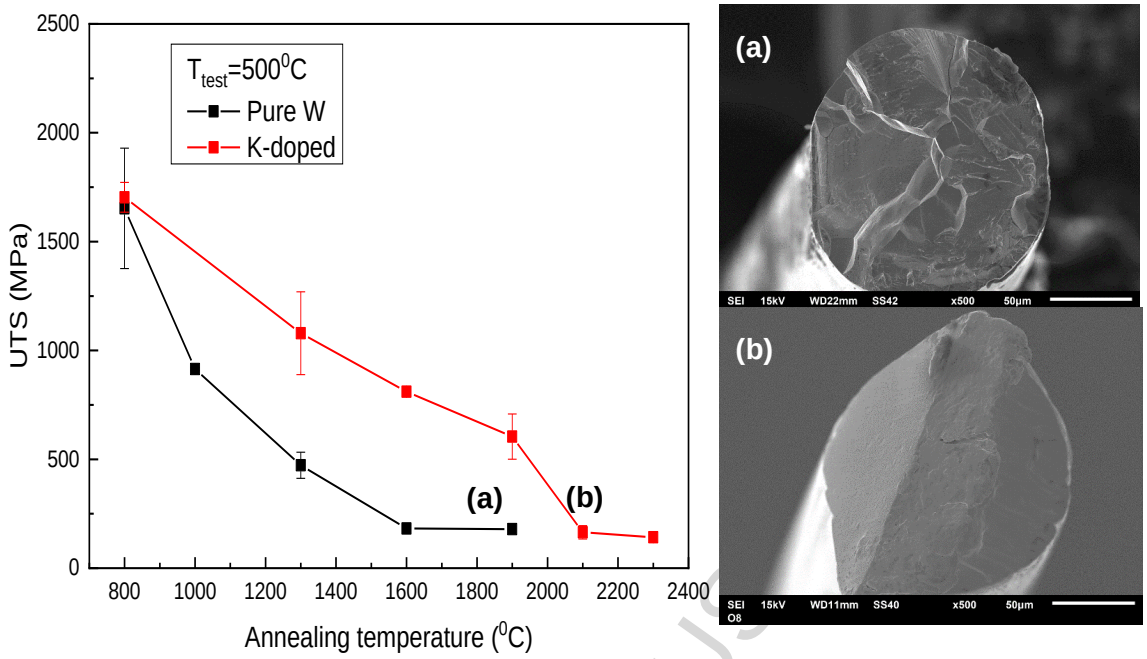

Fig.3. Ultimate tensile strength vs annealing temperature for wires tested at 500°C. Insets on the right show the fracture surface of (a) pure W wire annealed at 1900°C and (b) K-doped wire annealed at 2100°C. Results presented at T_a=800°C correspond to the as-fabricated state.

3.2 EBSD microstructure

3.2.1 Microstructure of pure W wire

Fig. 4 shows Inverse Pole Figure (IPF) maps of pure W wires in the as-received and annealed conditions. The color code is taken parallel with respect to an arbitrary radial direction (RD) to ease the appreciation of the grain shape and size as it evolves with increasing annealing temperature.

In the as-received condition, Fig. 4 (a), highly elongated grains can be noticed. These grains are up to 46 µm long and 4.3 µm wide, as obtained by the image post-processing analysis. While Fig.4(a) shows only central part of the wire, Fig.4 (b), (c) and (d) show the full width of the wire. Annealing at 1300°C, see Fig. 4 (b), already causes certain morphological changes of the grains. Annealing at 1300°C yields the average grain length to be almost 2 times larger compared to the as-received condition, whereas the width is almost 8 times larger. As the annealing temperature further increases, grains start to grow and tend to become equiaxed. At 1600 °C, the maximum size of the grains reaches 97 µm in length and 33 µm in width, while at 1900°C some grains occupy more than half of the wire diameter.

The distribution of both grain length and width, combined with the corresponding average values for each condition, are shown in Fig. A1 in the Annex 1 as individual histograms. One should note that these distributions are number fraction based and that the grains not entirely fit in the measured

ACCEPTED MANUSCRIPT

area are not incorporated in the delivered distribution. For the sake of brevity, here the size distribution is summarized as a single plot, which is shown in Fig.5(a).

Fig. A1 shows that the grains have essentially elongated shape, especially in the as-received and annealed at 1300°C conditions, which is in line with the pattern of the IPF maps (Fig. 4). Fig.5(a) summarizes the size distributions in as-received and annealed conditions in log scale as it facilities the appreciation of the annealing effect. One can see that the size distribution shifts from 1-10 µm range at 1300°C, to 10-100 µm range at the annealing temperature of 1900°C. Thus, two annealing stages causing significant changes in the grain size distribution are evident.

Based on Figure 4, up to 1600°C the grains seem to grow uniformly, after recrystallization, while at 1900°C the sample presented a non-homogeneous grain growth where some grains might have grown by accommodating smaller neighboring grains [36].

To make a deeper analysis of the modification of the texture as a result of the annealing, Pole Figures (PF) were plotted. Fig. 6 displays the PFs in the as-received and 1900°C annealed condition. One can see a very strong texture in <110> direction i.e. parallel to the Drawing Axis (DA) for both studied conditions, which is in a good correlation to the analyses performed in [27]. Strong <110> texture is indeed expected for the cold-drawn materials [37], regardless of the annealing temperature. The strongest texture intensity is naturally present in the as-received condition, see Fig.6 (a). The occurrence of grains with <110>//DA orientation is about 16 times higher than the random expectancy. After annealing at 1900°C it decreases down to 12, which is still rather high. To understand better the reasons for the remaining texture, we have also analysed the Grain Boundary Character Distribution (GBCD) and the Coincidence Site Lattices (CSL) boundaries. The results are shown in Fig.7 (a) and (b), respectively. The number fraction of CSLs (Σ3-Σ29) were determined according to Brandon's criterion from a maximum permissible deviation given by an equation of the form $\Delta\theta=\theta_0(\Sigma)^{-n}$ where θ=15 and n=0.5 and Σ is the reciprocal number density of lattice sites that are common, or coincident, between two neighboring grains [38]. Low angle grain boundaries (LAGBs) are referred here as those with misorientation angle below 15°, whereas the misorientation angle of high angle grain boundaries (HAGBs) exceeds 15°.

Fig.7 (a) shows that with the rise of the annealing temperature up to 1600°C, the fraction of LAGBs increases and fraction of HAGBs goes down. At 1900°C this trend is reversed. On the other hand, the fraction of CSL boundaries decreases monotonically. Usually, the most common deformation processes that are applied to polycrystalline metals (i. e. rolling and forging) are responsible for introducing LAGBs in the microstructure to store energy (of externally applied work) that becomes the driving force for recrystallization and grain growth under subsequent annealing [36]. The observation of the high fraction of HAGBs in the as-received and 1300°C annealed conditions (being around 50%) is not common for a highly deformed materials but was also observed for highly deformed W wires before [27]. In that study, the fraction of LAGBs was seen to growth under annealing up to 1100°C, while above 1300°C HAGBs were seen as dominant types of interfaces. Our results also show that HAGBs prevail over LAGBs, although here we perform more detailed decomposition to include CLS boundaries, which is probably why the absolute values for the fraction of LAGBs and HAGBs differ between the two works. According to a detailed study carried out by Hughes and Hansen [39] deformation inducing HAGBs is ascribed to continuous grain subdivision mechanisms that form crystallites surrounded by dislocation-wall boundaries resulting in large orientation spread based on dislocation accumulation processes. The reduction of HAGBs area fraction after the annealing is a consequence of orientation pinning and the strong texture developed by the W wires (as already shown in Fig. 6), where a growing grain meet a deformed crystallite with similar orientation leading to the replacement of a mobile HAGB by a slow moving

ACCEPTED MANUSCRIPT

LAGB interface. Zahid et al.[40] observed similar GBCD evolution in Al-alloys with a nanoscale lamellar HAGB structure and also Chen et al.[41] in cold-drawn Ti-Nb wires. Our observations provide a similar picture.

Fig.7 (b) shows that the CSL number fraction monotonically decreases with the annealing temperature going up. Several special boundaries, such as Σ3, Σ9, Σ11, Σ19a and Σ27a, clearly dominate other types. It is interesting to notice that the same type of predominance was also reported by Watanabe et al.[42], who studied the annealing of BCC Fe-6.5%Si ribbons with a strong <110> texture i.e. a very similar case of the initial microstructure.

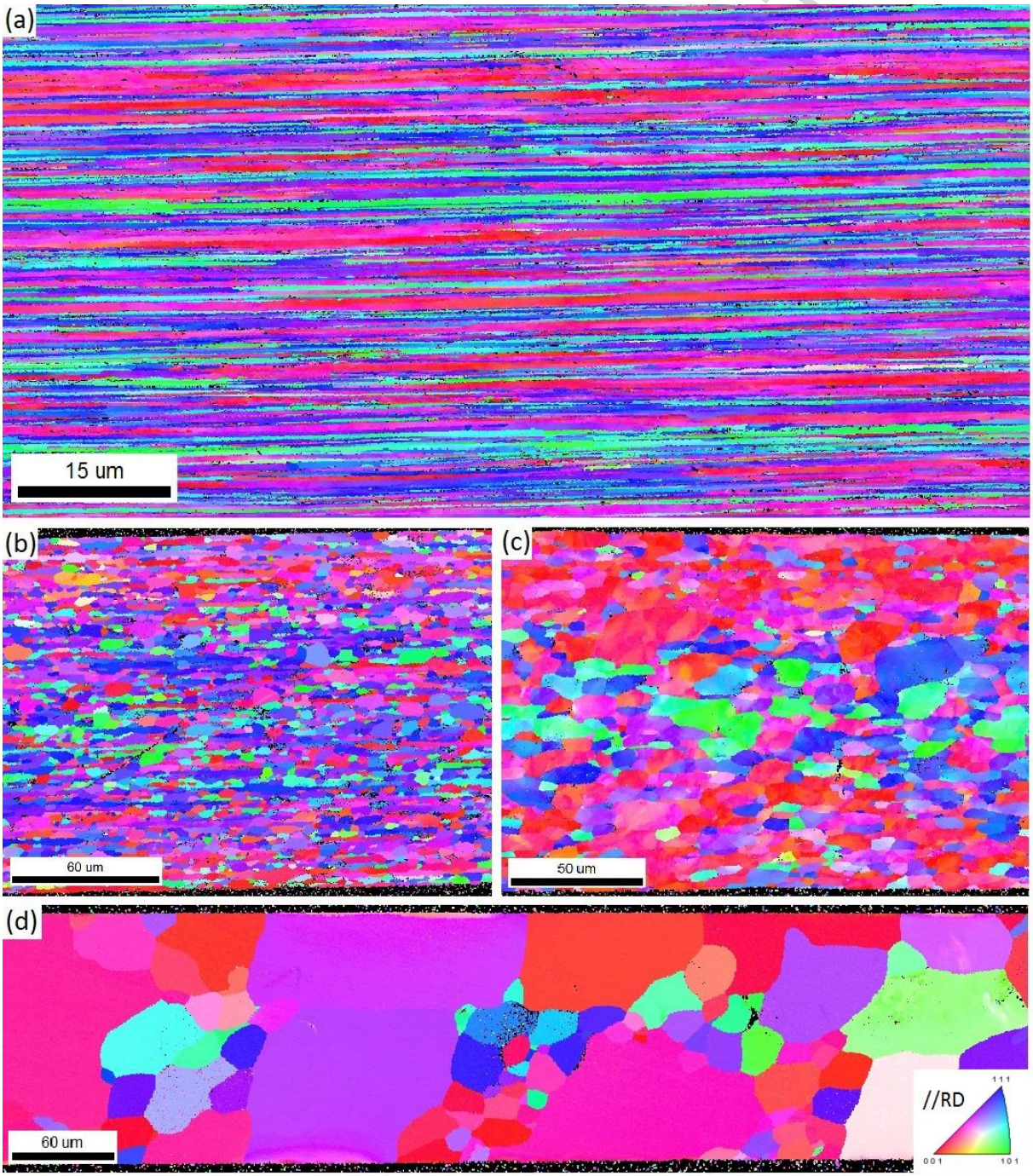

ACCEPTED MANUSCRIPT

Fig.4. Inverse Pole Figure maps of pure W wire in the (a) as-received, (b) annealed at 1300°C, (c) 1600°C and (d) 1900°C conditions. Colours represent crystallographic directions with respect to the rolling direction (i.e. drawing axis), according to the color code unit triangle.

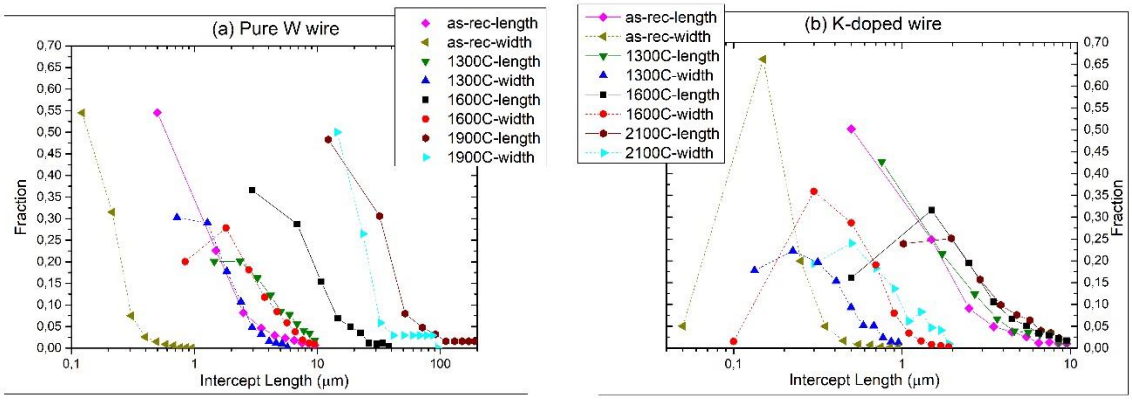

Fig.5. Distribution of the length and width of the grains measured in (a) pure and (b) K-doped wire.

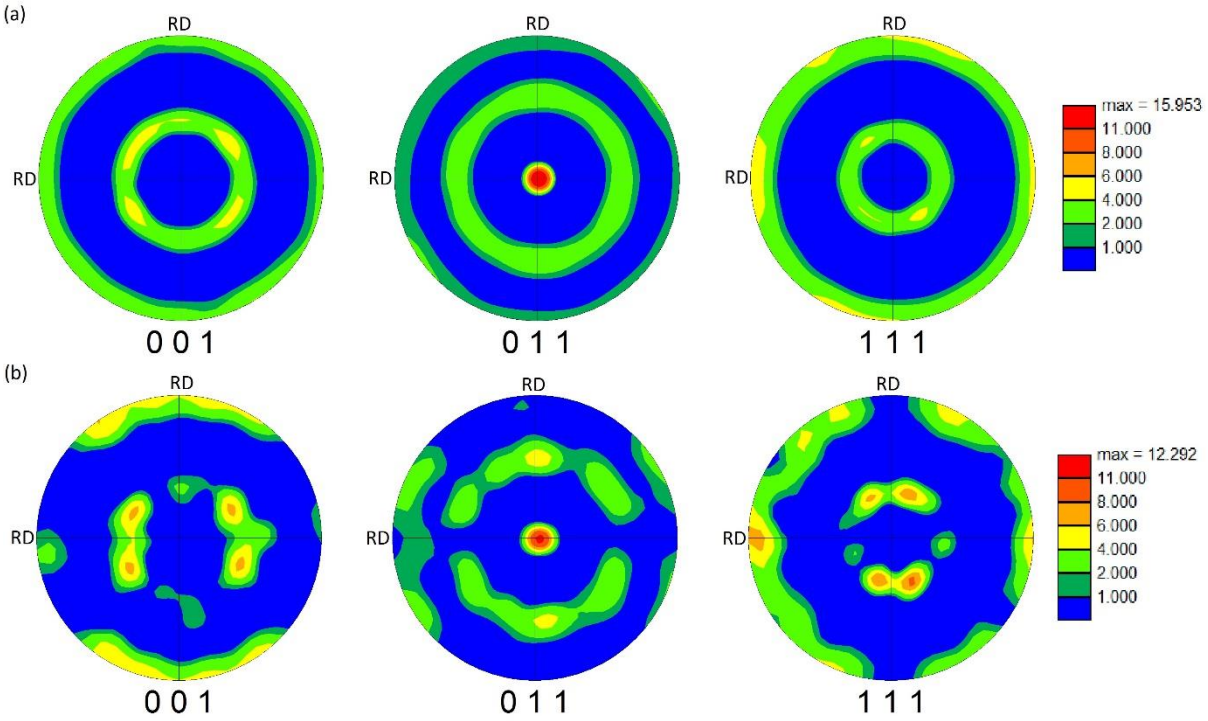

Fig. 6. Pole Figures of the pure W wire in the (a) as-received and (b) 1900°C annealed conditions. Drawing Axis is perpendicular to the paper. RD stands for Radial Direction.

ACCEPTED MANUSCRIPT

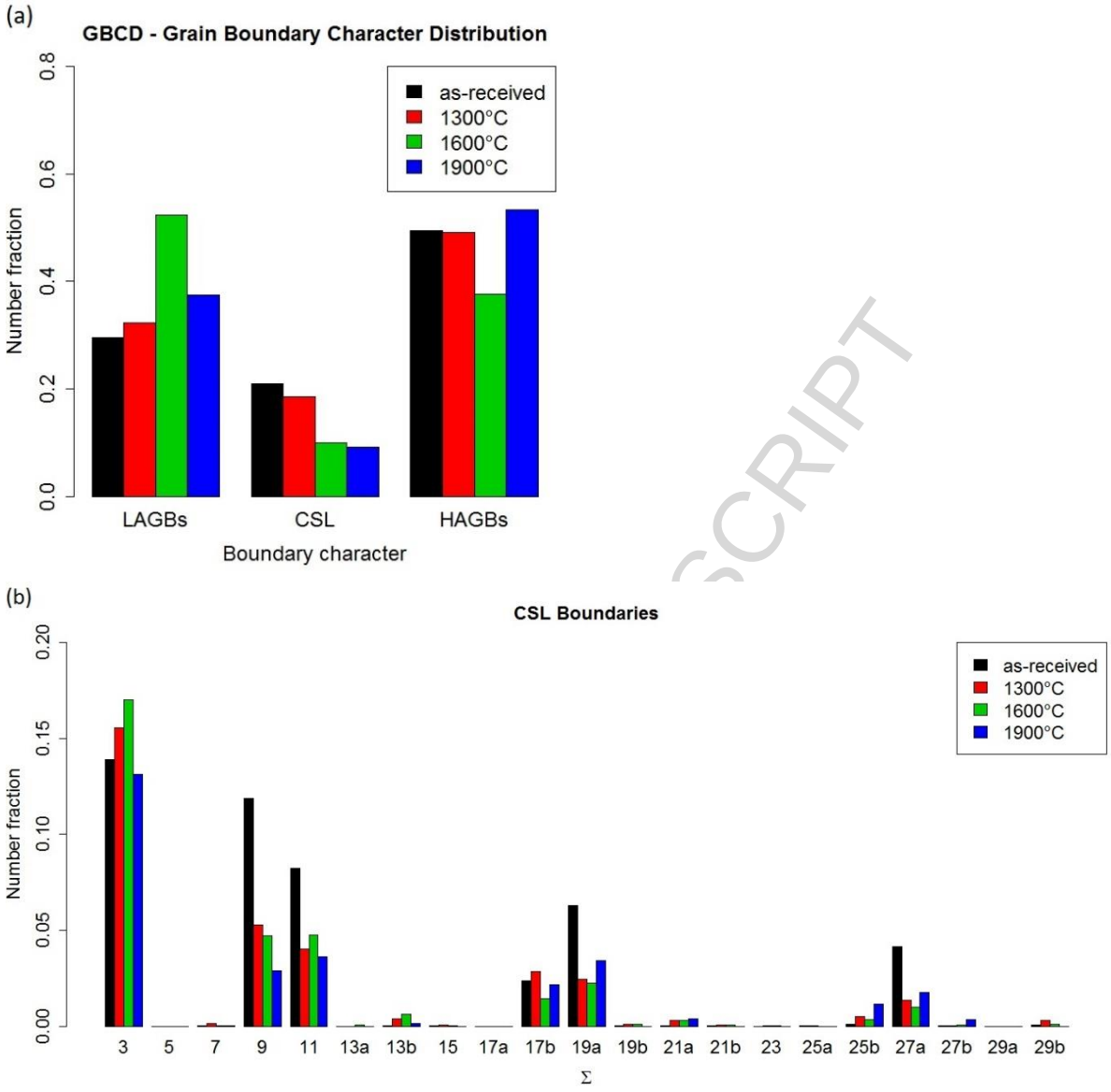

Fig.7. (a) Grain Boundary Character Distribution and (b) Coincidence Site Lattices distribution of the pure W wire.

3.2.2 Microstructure of K-doped wire

The same EBSD analysis as for pure W wire was applied for K-doped wire. IPF maps, Pole Figures and Grain Boundary Character distributions are presented in Figs. 8, 9, 10 and 11, respectively.

Below, we summarize the results in comparison with the data obtained in the pure W wire. IPF maps, presented in Fig.8, show that the microstructure of the K-doped samples annealed up to 1600°C is composed of thin elongated grains, practically resembling the microstructure of the as-received wire. Note that the microstructure of the pure and K-doped wire in the received state is very similar.

In the as-received K-doped sample, the grains are up to 47 µm long and 3 µm wide. These values change to 95 and 5 µm in the 1300°C annealed condition and reach up to 150 and 6 µm after annealing at 1600°C. Fig.8 (d) shows the grain pattern after annealing at 2100°C, which appears to be

ACCEPTED MANUSCRIPT

strongly different from the other IPF maps. The microstructure contains a few very elongated grains (longer than 900 μm) with some regions of smaller and stretched grains in between. Since the microstructure of the 2100°C annealed sample is more complex compared to the other samples, high resolution scans were made in specific regions to provide more information. IPF maps inside the two rectangles, labeled on Fig.8 (d) as A and B, are shown in Fig. 9 with a higher resolution where the grain length and width is 8.3 and 1.0 μm, on average, respectively. This result shows that besides the exaggerated grain growth proven by the existence of a few very large grains (observed across the whole EBSD scanned area), the small grains still present showing a very similar size distribution compared with the lower annealing temperature conditions. Evidently, the outer part of the wire is recrystallized, while the secondary recrystallization in the central part of the wire is not yet completed.

Fig. A2 in Annex 1 presents the detailed information on the length and width distributions of the grains for all studied conditions. In the case of the wire annealed at 2100°C, Figs. A2 (g) and (h) represent analysis of the small grains contained in the rectangle B on Fig. 8 (d). Indeed, due to the secondary recrystallization, the analysis of the whole EBSD scanned area does not make sense. Further, when referring to the analysis of 2100°C annealed sample, we imply the analysis of the small region shown in Fig.9. The distribution of the length and width of the grains collected for all the studied conditions is shown in Fig.5(b). The limited grain growth after the annealing at 2100°C can be seen.

Following the results obtained from the IPF maps, the annealing of K-doped wire leads to the observation of relatively uniform structural coarsening (primary recrystallization and normal grain growth) up to 1600°C (slow increase of both length and width of grains) which is followed by the abnormal grain growth (also known as secondary recrystallization) after annealing at 2100°C.

Fig.10 shows Pole Figures (PF) for as-received and 2100°C annealed K-doped samples (i.e. of the regions shown in Fig.9). As in the case of pure W sample, a very strong texture of <110> // DA type is evident in both studied states and 2100°C annealing practically does not change the texture intensity, which remains around 16.

Fig.11 displays GBCD and CSL distributions. As defined for pure W wire, the LAGBs comprise misorientation angle between 2 and 15°, whereas HAGBs refer to the misorientation angle exceeding 15°. One can see a slight reduction in the fraction of both LAGBs and HAGBs at expense of growing fraction of CSL interfaces. Since the CSLs represent GBs with the misorientation angle larger than 15°, the trend observed corresponds to the evolution expected in polycrystalline metals upon annealing i.e. the increase of HAGBs fraction and reduction of the LAGBs fraction [36]. The high fraction of HAGBs found irrespective of the annealing temperature (being around 45%), even in the as-fabricated condition, can be explained in terms of the grain subdivision mechanism due to the severe cold deformation. This mechanism would operate with and without K-doping and therefore both wires have similar as-fabricated microstructure. As described in details by Hughes and Hansen[39], grains and sub-grains surrounded by dislocations boundaries keep being submitted to continuous deformation resulting in large orientation spread due to dislocation accumulation processes. On the other hand the increase in the number fraction of CSL with the annealing temperature opens the possibility to improve some mechanical properties through grain boundary engineering as already done with other materials [43]. A closer look at Fig. 11(b) allows one to identify the main components of the CSL distribution. The formation of Σ3, Σ9, Σ11, Σ17b, Σ19a and Σ27a types of GBs is clearly dominant, which is also the case of pure W wire. The annealing-induced evolution of the fraction of the boundaries of Σ3, Σ9 and Σ27a type (i.e. increase in Σ3 and consequent reduction in both Σ9 and Σ27a) is in accordance with the "*Σ3 regeneration model"* described by Randle[43] where

ACCEPTED MANUSCRIPT

the interaction between boundaries at the triple junctions promotes the formation of Σ3 through the grain boundary conversion reaction of a kind $\Sigma3^{n} + \Sigma3^{n+1} = \Sigma3$. Naturally, this reaction is driven by the minimization of the interface energy and mis-orientation strains (i.e. Σ3 interface has the lower energy and strain misfit compared to Σ9 and Σ27a types), although the model was proposed for the metals with low stacking fault energy, it appears to be applicable also for tungsten, being the BCC metal with rather high stacking fault energy [44].

After in-depth representation and discussion of the microstructural features of the both types of wires, we can summarize the most important features of grain patterns and its evolution with annealing temperature. Fig.12 depicts the mean interception grain length as a function of annealing temperature for both longitudinal (i.e. length) and transversal (i.e. width) orientations of the grains. We see that in the as-received state, there is no essential difference between pure and K-doped wire, which is expected given the same fabrication procedure. However, under annealing the mean interception length in the pure W wire increases much steeper reaching 3-10 µm at 1600°C, while being 2-4 µm in the K-doped wire. After annealing of the pure W wire at 1900°C, the grain shape becomes more uniform (i.e. much less elongated). Contrary to that at 2100°C, in the K-doped wire, in its central part, the mean intercept length is 8 and 1 µm for length and width, respectively, while the outer part of the wire (30 µm from the surface) is fully recrystallized. Let us go back to Fig.8(d), which shows that the 2100°C annealed K-doped wire is made of two single grains composing outer and core parts of the wire, and being connected by the region containing fine elongated grains. The thickness of this "transition" region varies in the range of 10-30 µm. Clearly, the existence of this transition region as well as the mis-orientation of the outer and core region grains could help the wire to retain rather high strength at room temperature (see. Fig.1) and yields to the specific pattern of the fracture surface observed after the deformation at elevated temperature (Fig.3).

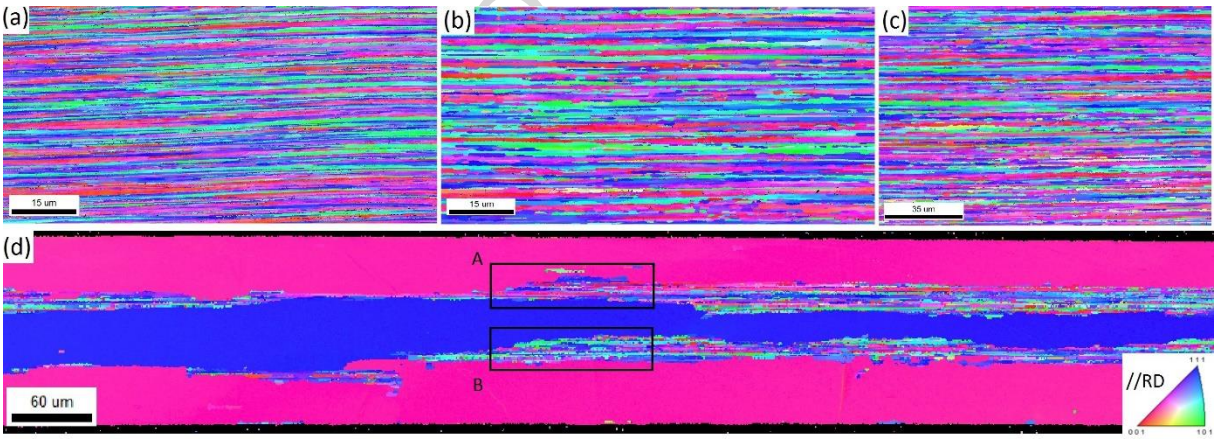

Fig.8. IPF maps for K-doped wire in the (a) as-received, (b) annealed at 1300°C, (c) 1600°C and (d) 2100°C conditions. Colours represent crystallographic directions with respect to the rolling direction (i.e. drawing axis), according to the color code unit triangle.

ACCEPTED MANUSCRIPT

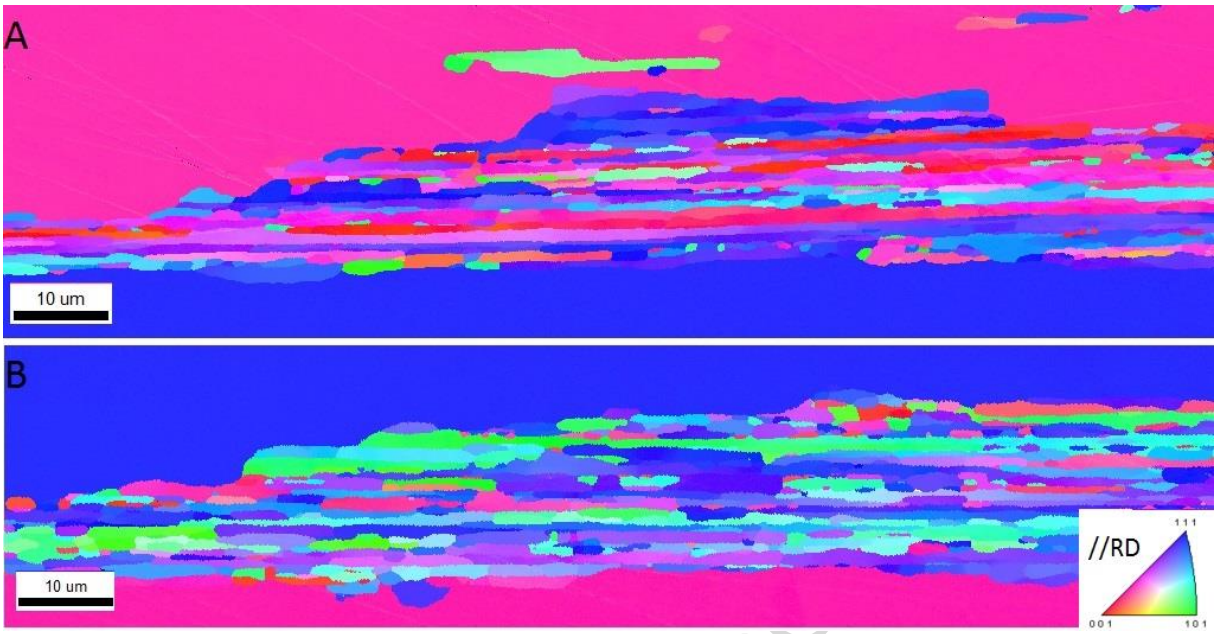

Fig.9. IPF maps of the selected areas specified in Fig. 8 (d). Colours represent crystallographic directions with respect to the rolling direction (i.e. drawing axis), according to the color code unit triangle.

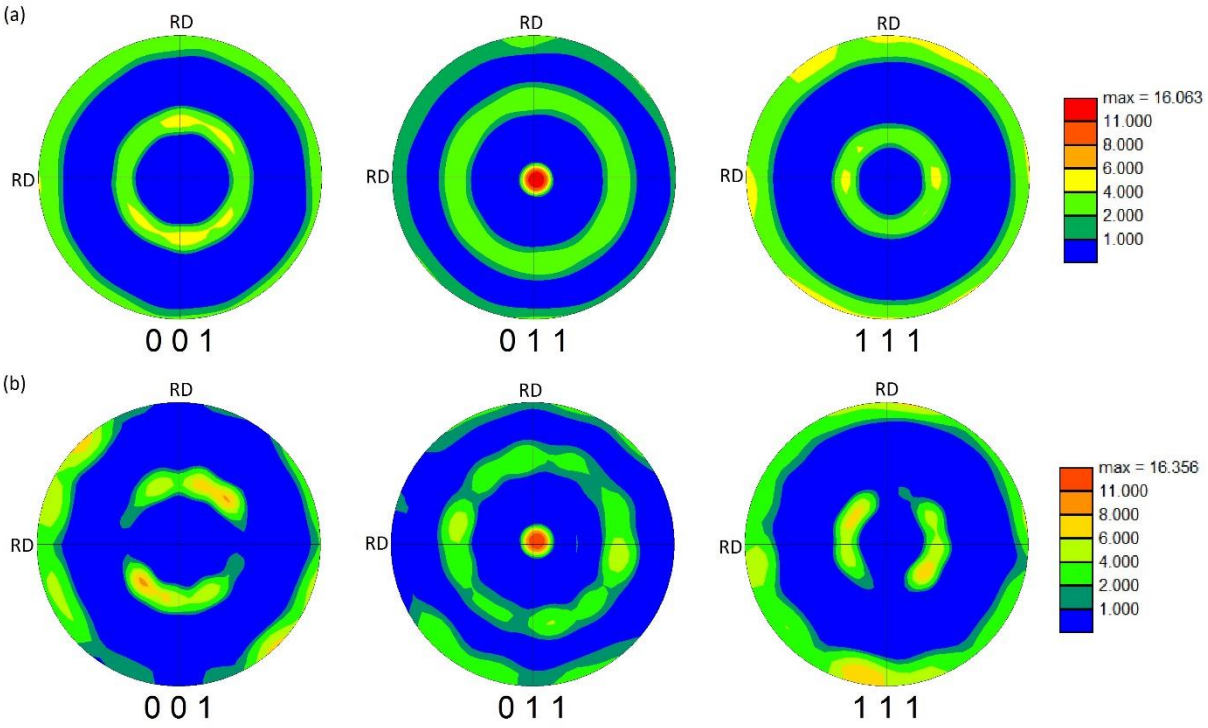

Fig. 10. PFs of the K-doped wire in the (a) as-received and (b) 2100°C annealed conditions. Drawing Direction is perpendicular to the paper. RD refers to Radial Direction.

ACCEPTED MANUSCRIPT

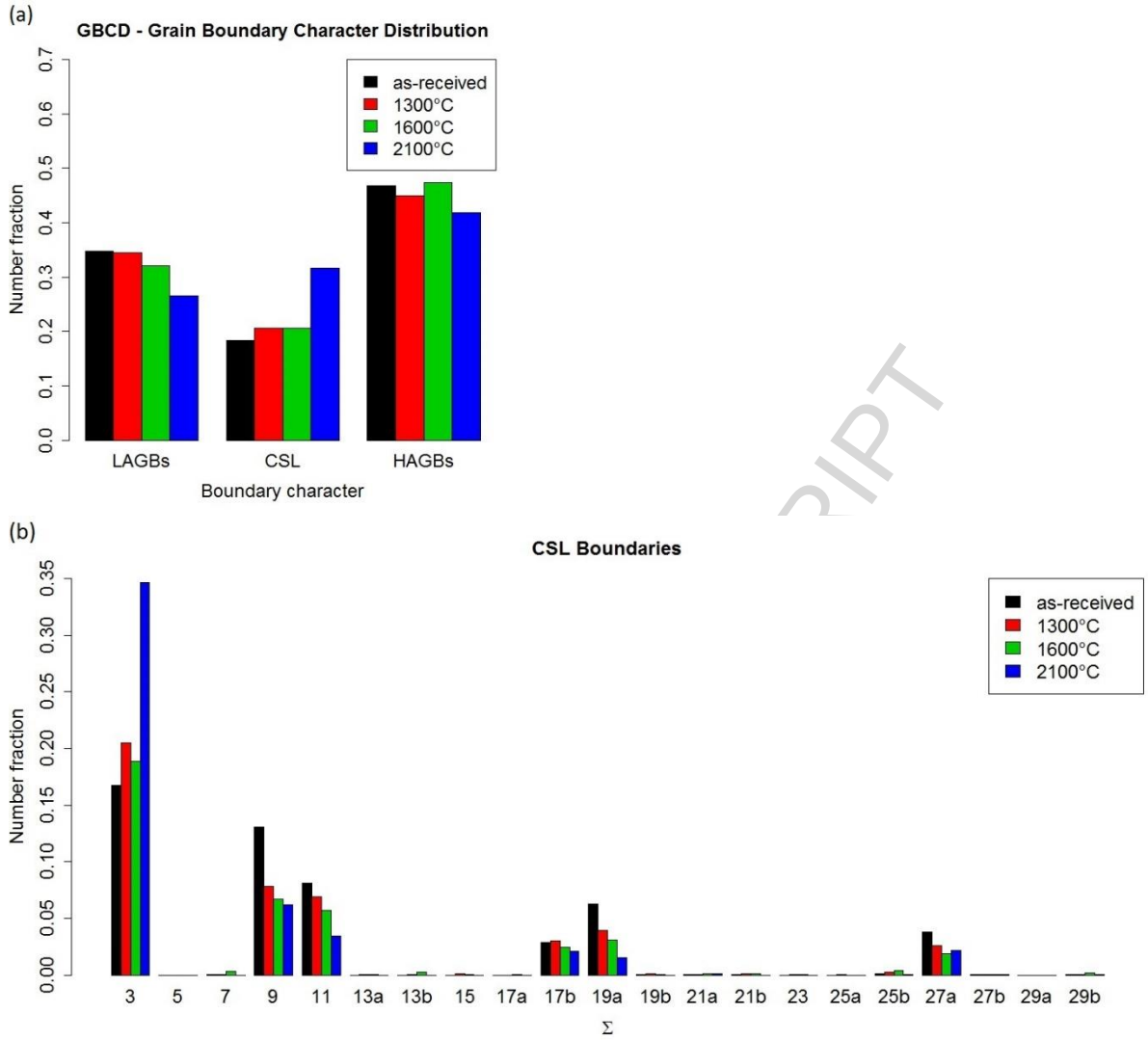

Fig. 11. (a) Grain Boundary Character and (b) Coincidence Site Lattices distributions for the K-doped wire.

ACCEPTED MANUSCRIPT

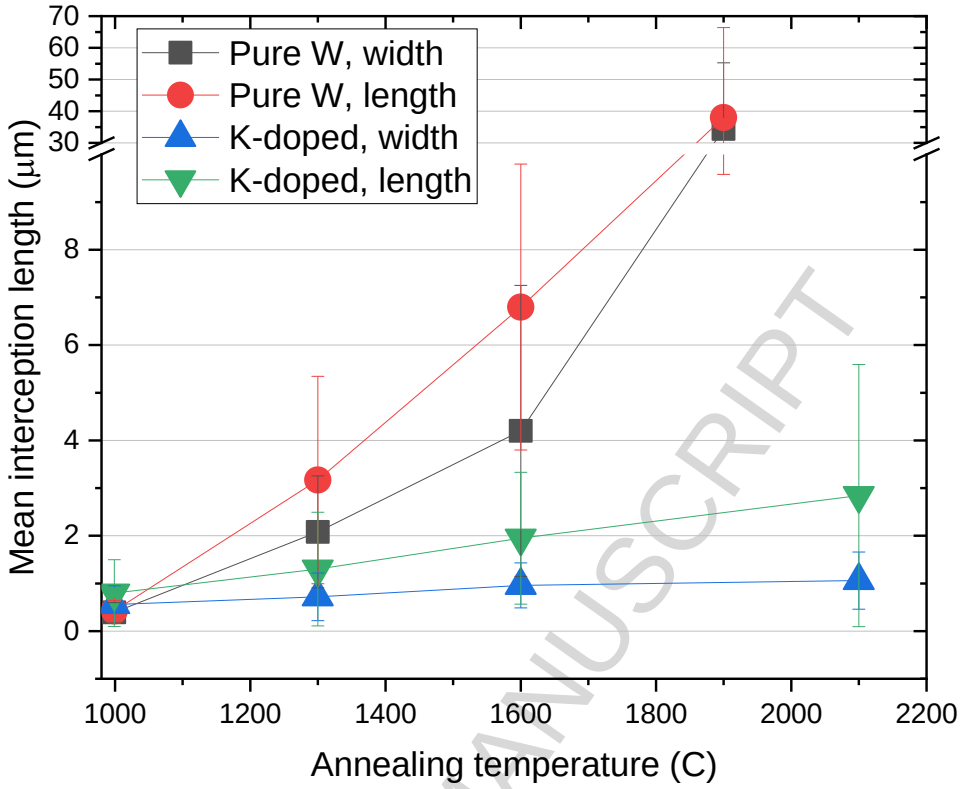

Fig.12. The effect of annealing on the increase of the mean interception length and width of the grains as obtained by EBSD analysis in pure W and K-doped wires.

3.3 Fracture surface

After representation of the grain structure it is easy to rationalize the fracture surface observed within the explored deformation and annealing temperatures. It is to be recalled that pure W wire annealed at 1900°C and K-doped annealed at 2300°C exibit premature fracture without yielding hence fracture surface is purely brittle. For the rest of the tested matrix, the typical patterns of the fracture surface are presented in Figs. 13 and 14. Let us start from the pure W wire i.e. Fig.13. In the as-fabricated state, the necking area is similar to a bullet shape and the reduction area increases with the test temperature, as expected. After annealing at 1000°, we see that RT deformation mechanism remains the same as for the as-fabricated wires – i.e. delamination via multiple cracks reaching the surface. At elevated temperature, intensive plastic deformation is seen by the rotation of the wire as well as the formation of longitudinal large cracks propagating across the wire's surface. At 1300°C, the grains grow considerably and this changes the fracture mechanism from delamination to trans/intergranular cleavage obtained in the deformation at room temperature. At elevated tempeature, the necking occurs with a considerable reduction area. At 1600°C, the grains are getting close to be equiaxed, yet the full recrystallization is not yet reached. The fracture surface is dominated by the intergranular fracture at both RT and elevated temperature. Finally, at 1900°C grains became very large and this leads to the one of the two types of the fracture surface: neck-to-edge or cleavage. The former one occurs if the necking is initiated in the region containig large single

ACCEPTED MANUSCRIPT

grain, the latter takes place if the necking region is close to the grain boundary interface, whose presence causes cleavage fracture.

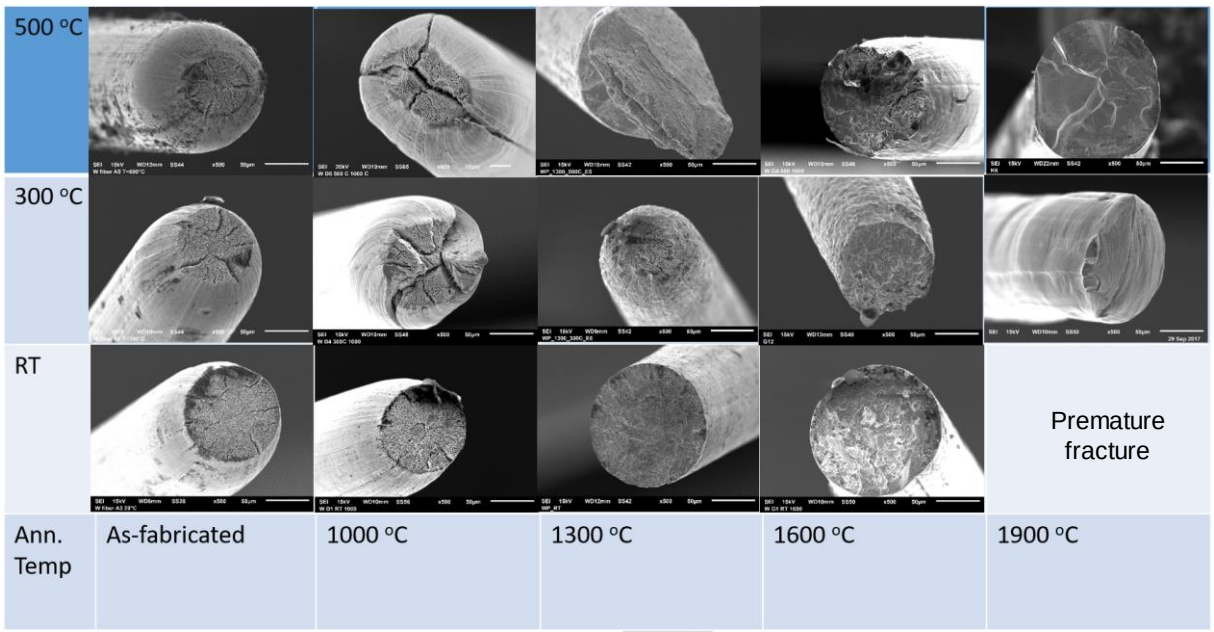

Fig.13. Typical fracture surfaces observed after the deformation of pure W wire depending on test (left column) and annealing temperature (bottom row). Down-right corner is empty as the wire is fully brittle at this condition.

The evolution of the fracture surface in K-doped wire is very similar to the pure W wire, except that the threshold temperature for the neck-to-edge deformation is shifted to 2300°C. Up to 1900°C, the deformation occurs by delamination and multipe crack propagation, since the fine structure of elongated grains is preserved thanks to K-doping. At 2100°C, quite specific fracture surface, determined by the presence of non-recrystallized transition region (see Fig.8d), appears at elevated temperature. Neck-to-edge deformation occurs after anneling at 2300°C. Hence, the complete recrystallization and removal of fine-grain structure takes place in the temperature range 2100-2300°C.

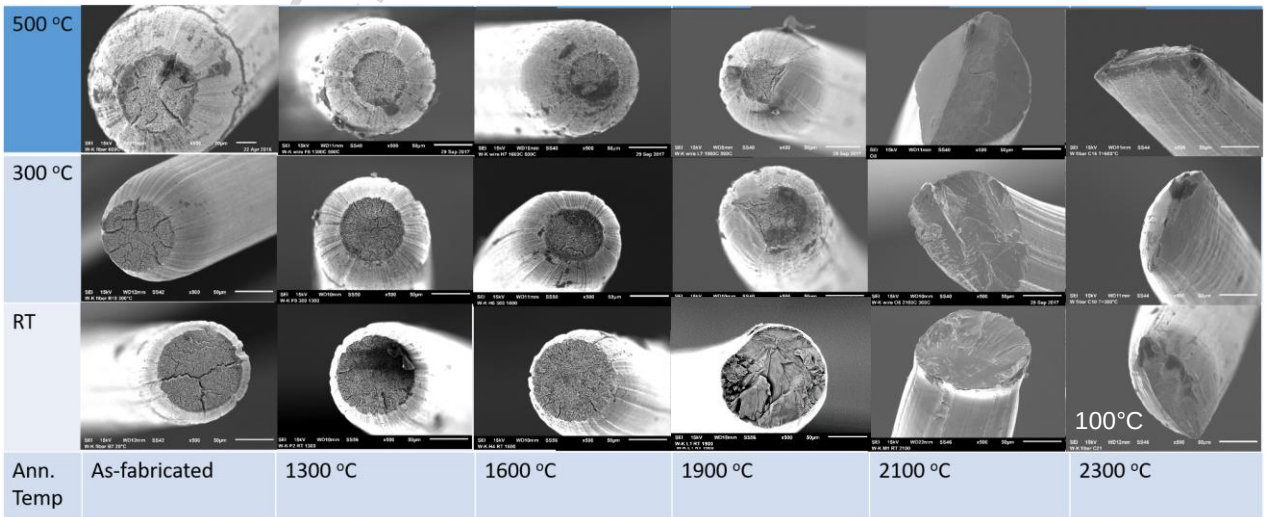

ACCEPTED MANUSCRIPT

Fig.14. Typical fracture surfaces observed after the deformation of K-doped wire depending on test (left column) and annealing temperature (bottom row). The fracture surfaces shown for T_{ann}=2300°C at RT (i.e. down right corner) correspond to the tests done at 100°C, as at RT the wire is fully brittle.

3.4 Nanoindentation tests

3.4.1 Hardness results

Nanoindentation tests were performed on the wires by positioning the head of the indenter in the centre of the wire. Examples of SEM micrographs showing the imprints of the indenter are given in Fig.15 and Fig.16 for pure and K-doped wires, respectively. Each figure shows the microstructure of the indented wire at two temperatures, which bound the interval at which the massive grain growth has occurred. Let us first discuss pure W wire. In Fig.15, we can see that the increase of the annealing temperature from 1600°C to 1900°C makes the grain size to grow from ~5 to ~50 µm. Thus, each indent in 1600°C annealed sample reflects the response of multiple grains, whereas in 1900°C annealed sample resistance to indentation is determined by a single or bi-grain structure. The second grain affected by indentation could be just next to or underneath the primary indented grain. In this situation, the measured hardness should be impacted (increase) by the interaction of the pile-ups formed underneath the crack tip with the grain boundary.

Fig.16 shows the pattern of indents on the 1900°C and 2100°C annealed K-doped samples. The 1900°C annealed sample keeps the fine structure of elongated grains, which is well seen in Fig.16(a). Each indent output is reponse of tens of grains. The sample annealed at 2100°C represents quite specific grain microstructure which is also shown in Fig.8(d) as EBSD scan. Central and outer parts of the wire are recrystallized, while the transition region between those two parts still contains fine-scale elongated grains, see Fig.9. The indentation was made in the central part of the wire, however, the spread of the plastic zone underneath the indenter very likely reached the transition region. Therefore, we do not expect to observe just a single-grain response but rather to see a contribution from the presence of the transition region as well.

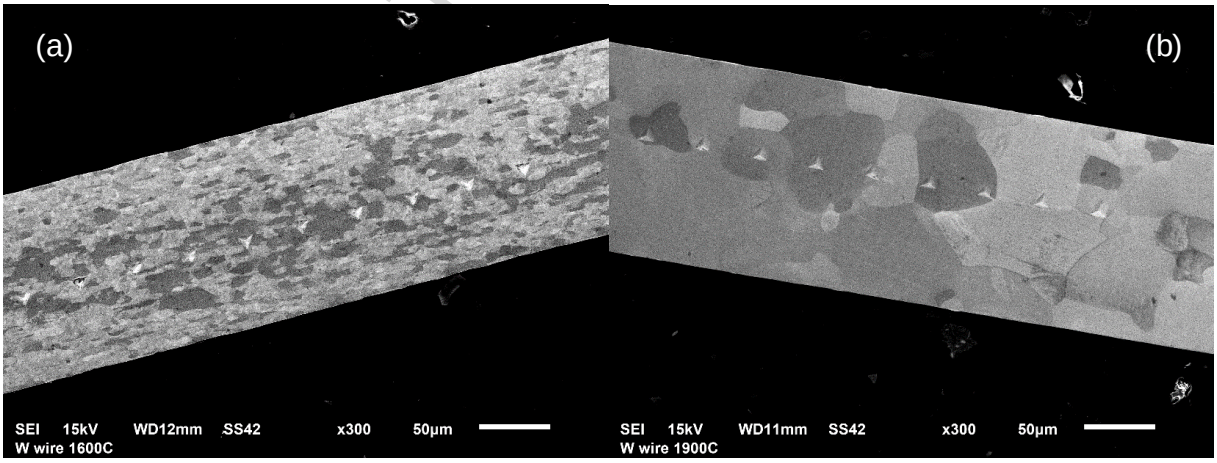

Fig.15. SEM micrographs of the imprints of the indenter in (a) pure W wire annealed at 1600°C and (b) pure W wire annealed at 1900°C.

ACCEPTED MANUSCRIPT

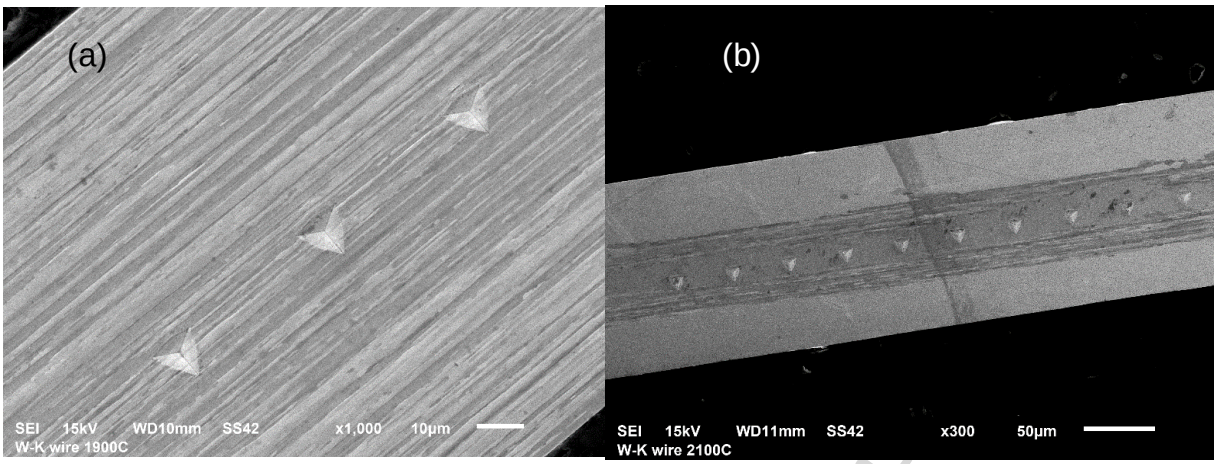

Fig.16. SEM micrographs of the imprints of indenter in (a) K-doped wire annealed at 1900°C and (b) K-doped wire annealed at 2100°C.

The hardness-depth curves calculated from the nanoindentation testing are shown in Fig.17 (a) and (b) for pure and K-doped wire, respectively. The x-axis on Fig.17(b) is reverted to enable easier comparison of the hardness at maximum depth (which will be referred as "saturated hardness", H_0). While the maximum indentation depth, *d*, is set as 1.4 µm (which is usual practice), the actual response of the material to the penetration of the indenter extends to the region of a factor of ~5 larger as it has been recently investigated by finite element analysis applied for tungsten [45]. Hence, we are exploring the response of the microstructure within the region of 5-7 µm underneath the indenter.

At a shallow depth, below ~200 nm, strong reduction of the hardness is observed which is called "size-effect" well known phenomenon originating from the transition of the material's response being dominated by production of geometrically necessary dislocations (GNDs) at shallow depth, which changes to the interaction with statistically stored dislocations (SSD) at larger depth. The hardness measured at a large depth (say > 1 µm) should represents the material response and exhibits correlation with the macroscopic flow stress [46, 47], which will be clarified here for the wires. It can be readily seen from the results shown in Fig.17 that each curve exhibits monotonic decrease with the increase of the indentation depth. The value of the saturated hardness strongly depends on the annealing temperature and presence of K-doping.

Given that the nanoindentation of thin wires, as used here, is not a standard procedure, it is important to understand how the obtained results compare with the measurements performed using bulk sample and standard sample preparation procedure. H_0 values for the wires and bulk tungsten sample, annealed in equivalent conditions but at 1300°C, 1500°C and 1800°C, are summarized in Fig.18. EBSD maps and hardness-depth curves for the bulk W are provided in Annex II in Fig.A3 and A4, respectively, together with a brief description of the microstructure and reference to the work where it was investigated. From Fig.18 we note the following: (i) in the as-fabricated state, both wires exhibit considerably higher hardness than bulk W. This is expected since the deformation applied to the wires is much higher compared to the hot forging of the bulk W; (ii) with the increase of annealing temperature, H_0 linearly decreases, having a significant reduction already at 1300°C in both types of wires. Note that at 1300°C, no strong change in the grain microstructure was registered by EBSD in the K-doped wire. Hence, the reduction of H_0 must be attributed to the annealing of dislocations, which was observed in bulk W sample by transmission electron microscopy [32]; (iii)

ACCEPTED MANUSCRIPT

there is a good agreement for H_0 obtained in pure W bulk and wire, except for the as-fabricated state as discussed above. Given similarity in the microstructure (and purity of materials), this agreement supports the applicability/reliability of nanoindentation measurements applied to half-cut 150 µm wire. Indeed, indenting rather thin samples is not a standard procedure and a priori the response of the sample holder could have been expected; (iv) finally, the presence of K-doping clearly retards the reduction of the hardness with the increase of the annealing temperature compared to the pure W wire. Even after annealing at 2100°C, H_0 of K-doped wire is 5.91 GPa, which is comparable to 5.90 GPa of the pure W annealed at 1600°C. Thus, the results of nanoindentation unambiguously show the positive effect of K-doping, otherwise demonstrated by the investigation of microstructure and tensile properties.

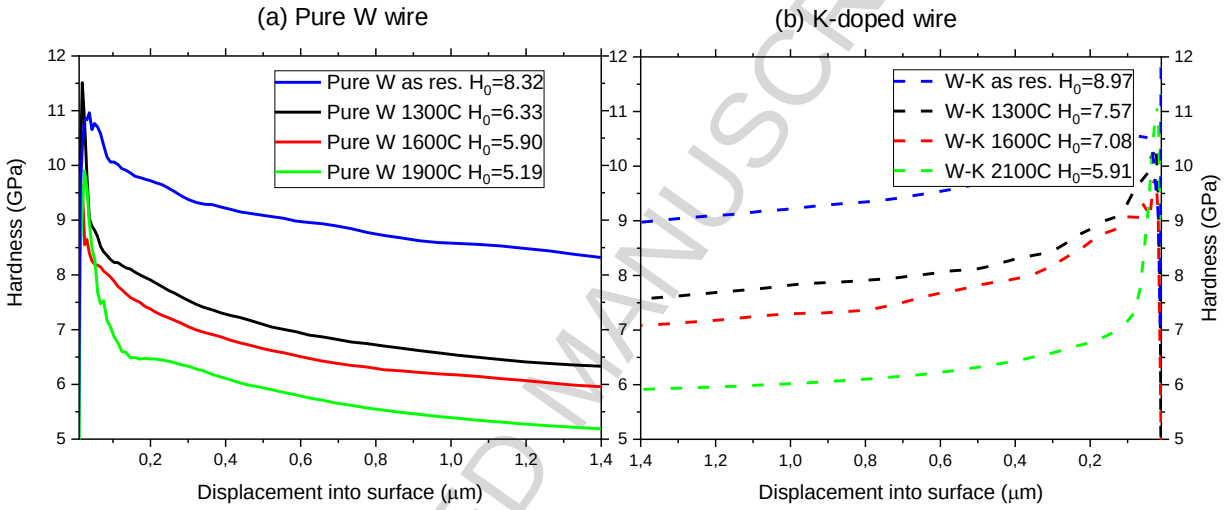

Fig.17. Hardness – depth relationship for (a) pure W and (b) K-doped wire measured in the central region of the wires. The annealing tempetures and saturated hardness (H_0, expressed in GPa) are shown on the legend.

ACCEPTED MANUSCRIPT

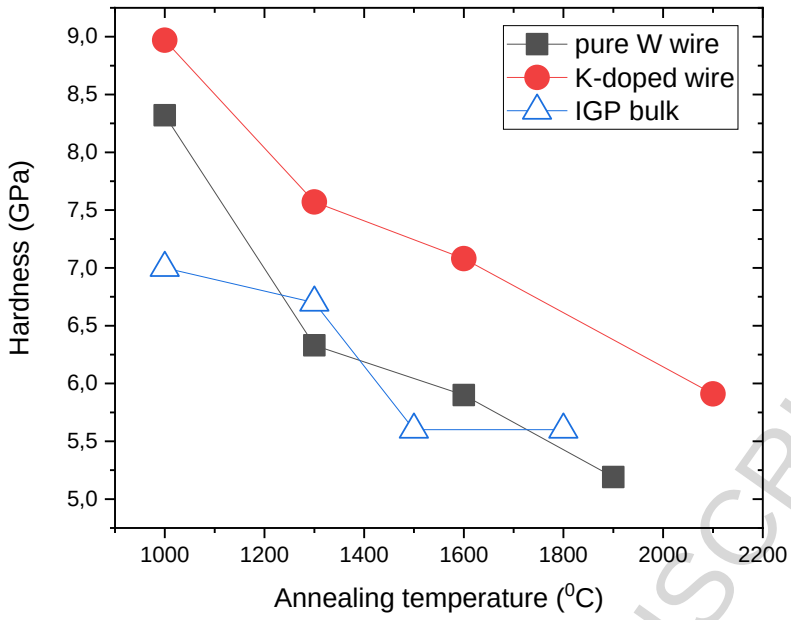

Fig.18. Saturated hardness measured in the wires and bulk forged tungsten depending on the annealing temperature. The error bars correspond to the size of the symbols. "IGP bulk" stands for bulk tungsten sample whose origin is explained in Section2.1.

3.4.2 Correlation between UTS and hardness measured by nanoindentation

Given that the hardness measured by nanoindentation testing should be related with the flow properties of the material, we made an attempt to establish a correlation of H_0 with the mechanical properties of the wires measured from the tensile tests [22, 24]. Since the extraction of the yield/proof stress for the wire is somewhat ambigous due to the lack of the standardized geometry and accuracy of the strain measurement, the most reliable (and important for the reinforcement application) mechanical property is the ultimate tensile strenght. The UTS for the wires studied here were established earlier in [24]. UTS versus H_0 (measured at RT !) is plotted in Fig.19 (a) and (b) for pure and K-doped wires, respectively. One can see that there is almost linear relation between H_0 and UTS, eventhough the UTS was measured not only at room temperature (i.e. same as H_0) but also at 300°C and 500°C. The linear relation breaks down only in the case of pure W wire annealed above 1600°C. This is when the wire completely loses the fine-grain structure and so its strength is determined by the necking proceeding via generation of dislocations from the wire surface and their glide. In all other cases, the plastic deformation of W wires was govered by the availability of grains and sub-grains which act as sources and obstacles for the dislocation motion, thereby controlling the macroscopic deformation of the wire and its UTS. Evidently, the application of nanoindentation to deduce H_0 allows one to establish a good correlation with the UTS by simply using a linear expression like $\sigma_{UTS}=A+B\times H_0$ (1). Based on the results presented in Fig.19, *A* and *B* are collected in Fig.20. *B* represents the slope of UTS in Fig.19 and is nearly constant (with temperature) being about 0.5 for the pure W wire and 0.65 for the K-doped W wire. *A* is an analogus of an off-set stress and it monotonically decreases with test temperature.

ACCEPTED MANUSCRIPT

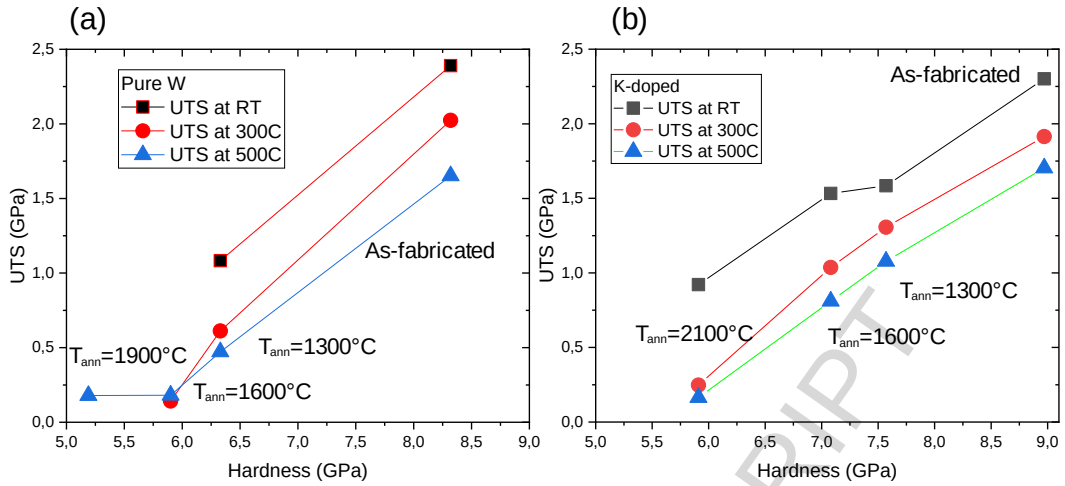

Fig.19. UTS vs. hardness for (a) pure W wire and (b) K-doped W wire. The annealing temperature is reciprocal to the hardess/UTS value.

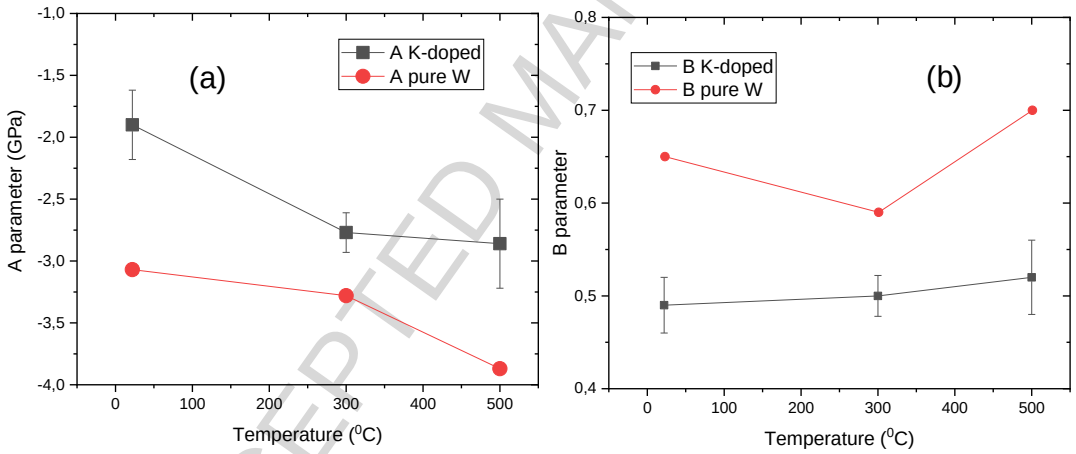

Fig.20. Best fit parameters for the linear expression of UTS as a function of hardness, i.e. $\sigma_{UTS}=A+B\times H_0$, obtained for pure W wire and K-doped W wire.

ACCEPTED MANUSCRIPT

4. Summary and conclusions

In this work, we have performed a combined experimental investigation of the impact of high temperature annealing on the micro-mechanical and microstructural properties of tungsten wires. Particular focus was put on the understanding of the role played by potassium doping in the recrystallization process occurring under annealing. The applicability of the standard nanoindentation with Berkovich type head to probe ultra-thin tungsten samples was also addressed in this work. The validity of the nanoindentation measurements was cross-checked using reference bulk tungsten samples in different annealing conditions. The parametric mechanical testing was performed using as-received and annealed wires in the temperature range 1300-2300°C and the

ACCEPTED MANUSCRIPT

results of tensile strength were reported in our previous work [24]. The present investigation included a systematic microstructural characterization of the fracture surface and grain morphology by EBSD scanning, as well as nanoindentation testing performed at room temperature.

In this study, the duration of the annealing was one hour. Hence, the presented here results and below provided summary reflect the impact of this particular duration of the annealing. It is important to keep in mind that longer annealing times (given that the process of grain growth follows the Arrhenius law) could change the situation, especially in the transition temperature region, which is determined to be above 1600°C for pure W wire, and above 1900°C for the K-doped wire.

On the basis of the obtained results and their discussion, we can summarize the statements regarding the mechanical properties, microstructure and nanoindentation testing as follows:

(i) the results of the tensile testing are summarized and analyzed together with the fracture surface patterns. In the as-fabricated state and at room temperature, both wires exhibit fracture by necking and the fracture surface consists of a numerous µm-size necked grains forming the so-called "knife edge pattern". It is shown that after annealing at 1600°C, in the tests at room temperature, pure W wire exhibits premature fracture which occurs by intergranular cleavage. K-doped wire exhibits necking up to 1600°C, and above this temperature the transgranular cleavage takes place. At elevated temperature, the wires annealed up to the highest temperature (pure W wire 1900°C, K-doped wire 2300°C) exhibit large plastic deformation resulting in the 100% reduction of the fracture surface (i.e. neck-to-edge fracture). K-doped wire annealed at 2100°C does not appear to have 100% of the reduction area and the central part of the wire shows flat cleavage surface pattern, suggesting that recrystallization was not completed after 2100°C annealing.

(ii) EBSD measured and post-processing analysis performed to calculate the effective grain size, characteristic length/width and grain texture has confirmed that K-doping strongly suppressed grain growth. In the case of pure W wire, two distinct stages of grain growth are observed after annealing to 1300°C (mean grain size increased from ~0.2 µm to ~2 µm) and to 1900°C (mean grain size increased from ~3 µm to ~27 µm). In the second stage of grain growth, the grains become fully equiaxed. In the K-doped wire, only one major stage of grain growth is observed to occur at 2100°C due to secondary recrystallization. The wire exhibits a bi-modal grain size distribution because the outer and central parts of the wire are completely recrystallized while the middle region contains small elongated grains with mean size ~1 µm. Such grain pattern fully explains why the 2100°C annealed wire exhibited cleavage fracture surface at room temperature and was half-necked at elevated temperature. The pole figures obtained for the as-fabricated and annealed wires show that both types of wires have strong <110> // DA texture which only slightly weakens after the annealing. It was also found that annealing does not have a very strong impact on the distribution of the character of grain boundaries. The major fraction of grain boundaries is of high angle type (~50 %), other ones are coincidence site lattice (CSL) and low angle grain boundaries. The specific analysis of the CSLs show that major fraction of GBs is of Σ3, Σ9, Σ11, Σ17, Σ19 and Σ27 in both types of wires. In the case of tungsten prepared via conventional routes (hammering), we observe that the fraction of CSL boundaries is significantly lower and that there are no preferential CSL's observed.

(iii) The saturated hardness (H_0), measured at the indentation depth of 1.4 µm, is found to progressively decrease with raising the annealing temperature. K-doping suppresses the reduction of the hardness, which is fully consistent with the evolution of the microstructure (i.e. grain pattern). The additional NI measurements performed using hot forged bulk tungsten (of the same purity) have shown a good agreement for H_0 measured in the pure W wire. The only considerable difference was registered for the as-fabricated material, naturally, since much heavier deformation was applied to

ACCEPTED MANUSCRIPT

the wires during the extrusion process. The obtained good agreement for H_0 on the annealed bulk and wire tungsten proves the robustness of the nanoindentation testing applied to thin half-cut wire samples. Finally, a good linear correlation between the ultimate tensile strength (UTS) and saturated hardness is found for both pure and K-doped tungsten wires as long as the ductility and strength are controlled by fine µm-sized grain microstructure. In the wires which exhibit complete recrystallization (i.e. pure W wire annealed at 1600°C and above) such correlation is absent. The observation of the rigorous correlation between H_0 and UTS opens a perspective to use NI testing for characterization of the irradiation or fatigue damage induced in the wires, which is needed to evaluate the capacity of the wires to operate in fusion environment where high energy neutrons are expected to degrade initially attractive mechanical properties achieved by the wire extrusion process. Besides, the ability to correlate NI hardness with the ultimate tensile strength is an important finding as it prompts an application of accelerated irradiation by heavy ions which allows one to reach high irradiation doses without activating the material but has essentially limited penetration depth, typically limited to few µm. As of today, nanoindentation method remains to be the main tool for characterization of the mechanical properties after ion irradiation.

Acknowledgements

This work has been carried out within the framework of the EUROfusion Consortium and has received funding from the Euratom research and training programme 2014–2018 under grant agreement No 633053. The views and opinions expressed herein do not necessarily reflect those of the European Commission. The work was partially supported by FOD grant of Belgium Government. The authors want to acknowledge support by Osram GmbH, Schwabmünchen, Germany for providing the tungsten wire and performing the annealing.

References

[1] S.J. Zinkle, J.T. Busby, Structural materials for fission & fusion energy, Materials Today 12(11) (2009) 12-19.
[2] M.R. Sanjay, G.R. Arpitha, B. Yogesha, Study on Mechanical Properties of Natural - Glass Fibre Reinforced Polymer Hybrid Composites: A Review, Mater Today-Proc 2(4-5) (2015) 2959-2967.
[3] J. Riesch, J.Y. Buffiere, T. Hoschen, M. di Michiel, M. Scheel, C. Linsmeier, J.H. You, In situ synchrotron tomography estimation of toughening effect by semi-ductile fibre reinforcement in a tungsten-fibre-reinforced tungsten composite system, Acta Materialia 61(19) (2013) 7060-7071.
[4] L.C. Zhuo, Y.H. Zhang, Q.Y. Chen, S.H. Liang, L. Chen, J.T. Zou, Fabrication and properties of the W-Cu composites reinforced with uncoated and nickel-coated tungsten fibers, Int J Refract Met H 71 (2018) 175-180.
[5] T.P. Sathishkumar, S. Satheeshkumar, J. Naveen, Glass fiber-reinforced polymer composites - a review, J Reinf Plast Comp 33(13) (2014) 1258-1275.
[6] Q. Sun, X. Luo, Y.Q. Yang, G.H. Feng, G.M. Zhao, B. Huang, A review on the research progress of push-out method in testing interfacial properties of SiC fiber-reinforced titanium matrix composites, Compos Interface 22(5) (2015) 367-386.
[7] S.F. Tang, C.L. Hu, Design, Preparation and Properties of Carbon Fiber Reinforced Ultra-High Temperature Ceramic Composites for Aerospace Applications: A Review, J Mater Sci Technol 33(2) (2017) 117-130.
[8] R. Neu, J. Riesch, A.V. Muller, M. Balden, J.W. Coenen, H. Gietl, T. Hoschen, M. Li, S. Wurster, J.H. You, Tungsten fibre-reinforced composites for advance d plasma facing components, Nuclear Materials and Energy 12 (2017) 1308-1313.
[9] C. Linsmeier, M. Rieth, J. Aktaa, T. Chikada, A. Hoffmann, J. Hoffmann, A. Houben, H. Kurishita, X. Jin, M. Li, A. Litnovsky, S. Matsuo, A. von Muller, V. Nikolic, T. Palacios, R. Pippan, D. Qu, J. Reiser, J.

ACCEPTED MANUSCRIPT

Riesch, T. Shikama, R. Stieglitz, T. Weber, S. Wurster, J.H. You, Z. Zhou, Development of advanced high heat flux and plasma-facing materials, Nuclear Fusion 57(9) (2017).
[10] S.J. Zinkle, J.T. Busby, Structural materials for fission & fusion energy, Materials today 12 (2009).
[11] A. Hasegawa, M. Fukuda, S. Nogami, K. Yabuuchi, Neutron irradiation effects on tungsten materials, Fusion Engineering and Design 89(7-8) (2014) 1568-1572.
[12] I.V. Gorynin, V.A. Ignatov, V.V. Rybin, S.A. Fabritsiev, V.A. Kazakov, V.P. Chakin, V.A. Tsykanov, V.R. Barabash, Y.G. Prokofyev, Effects of Neutron-Irradiation on Properties of Refractory-Metals, Journal of Nuclear Materials 191 (1992) 421-425.
[13] G. Pintsuk, Tungsten as a Plasma-Facing material, (2012).
[14] P. Schade, 100 years of doped tungsten wire (vol 28, pg 647, 2010), Int J Refract Met H 29(4) (2011) 559-559.
[15] C.L. Briant, E.L. Hall, The Microstructure of Rolled and Annealed Tungsten Rod, Metall Trans A 20(9) (1989) 1669-1686.
[16] C.L. Briant, B.P. Bewlay, The Coolidge Process for Making Tungsten Ductile - the Foundation of Incandescent Lighting, Mrs Bull 20(8) (1995) 67-73.
[17] E. Pink, L. Bartha, The metallurgy of doped/non-sag tungsten, Elsevier Science Publishers (1989).
[18] J. Riesch, T. Hoschen, C. Linsmeier, S. Wurster, J.H. You, Enhanced toughness and stable crack propagation in a novel tungsten fibre-reinforced tungsten composite produced by chemical vapour infiltration, Physica Scripta T159 (2014).
[19] J. Riesch, M. Aumann, J.W. Coenen, H. Gietl, G. Holzner, T. Hoschen, P. Huber, M. Li, C. Linsmeier, R. Neu, Chemically deposited tungsten fibre-reinforced tungsten - The way to a mock-up for divertor applications, Nuclear Materials and Energy 9 (2016) 75-83.
[20] P. Zhao, J. Riesch, T. Hoschen, J. Almanstotter, M. Balden, J.W. Coenen, R. Himml, W. Pantleon, U. von Toussaint, R. Neu, Microstructure, mechanical behaviour and fracture of pure tungsten wire after different heat treatments, Int J Refract Met H 68 (2017) 29-40.
[21] J. Riesch, A. Feichtmayer, M. Fuhr, J. Almanstötter, J.W. Coenen, H. Gietl, T. Höschen, C. Linsmeier, R. Neu, Tensile behaviour of drawn tungsten wire used in tungsten fibre-reinforced tungsten composites, Physica Scripta 2017 (2017) 014032.
[22] D. Terentyev, J. Riesch, S. Lebedev, A. Bakaeva, J.W. Coenen, Mechanical properties of as-fabricated and 2300 °C annealed tungsten wire tested up to 600 °C, Int J Refract Met H 66 (2017) 127-134.
[23] D. Terentyev, J. Riesch, S. Lebediev, T. Khvan, A. Zinovev, M. Rasiński, A. Dubinko, J.W. Coenen, Plastic deformation of recrystallized tungsten-potassium wires: constitutive deformation law in the temperature range 22-600°C, Int J Refract Met H 66 (2018) 127-134.
[24] D. Terentyev, J. Riesch, S. Lebediev, T. Khvan, A. Zinovev, M. Rasiński, A. Dubinko, J.W. Coenen, Strength and deformation mechanism of tungsten wires exposed to high temperature annealing: impact of potassium doping, International Journal of Refractory Metals and Hard Materials 76 (2018) 226-233.
[25] D. Terentyev, J. Riesch, S. Lebediev, T. Khvan, A. Dubinko, J.W. Coenen, EBSD maps of annealing tungsten wire: effect of pottasium doping on the recrystallization, International Journal of Refractory Metals and Hard Materials (2018) submitted.
[26] H.H. Jansen, Aspects of the recrystallization kinetics of doped tungsten, Philips J. Res. 42 (1987) 3-14.
[27] V. Nikolic, J. Riesch, R. Pippan, The effect of heat treatments on pure and potassium doped drawn tungsten wires: Part I - Microstructural characterization, Mat Sci Eng a-Struct 737 (2018) 422-433.
[28] O. Horacsek, C.L. Briant, K. Horacsek, Effect of heating rate on the recrystallization behaviour of doped tungsten, High Temp Mater Proc 16(1) (1997) 15-27.
[29] J. Riesch, Y. Han, J. Almanstotter, J.W. Coenen, T. Hoschen, B. Jasper, P. Zhao, C. Linsmeier, R. Neu, Development of tungsten fibre-reinforced tungsten composites towards their use in DEMO-potassium doped tungsten wire, Physica Scripta T167 (2016).

ACCEPTED MANUSCRIPT

[30] A. Dubinko, D. Terentyev, A. Bakaeva, K. Verbeken, M. Wirtz, M. Hernandez-Mayoral, Evolution of plastic deformation in heavily deformed and recrystallized tungsten of ITER specification studied by TEM, Int. Journal of Refractory Metals and Hard Materials 66 (2017) 105-115.
[31] D. Terentyev, G. De Temmerman, T.W. Morgan, Y. Zayachuk, K. Lambrinou, B. Minov, A. Dubinko, K. Bystrov, G. Van Oost, Effect of plastic deformation on deuterium retention and release in tungsten, J Appl Phys 117(8) (2015) 083302.
[32] A. Dubinko, Plastic Deformation of Tungsten under Fusion-Plasma Exposure Conditions, PhD thesis, University of Ghent (2017) ISBN 978-94-6355-127-4.
[33] W.C. Oliver, G.M. Pharr, Measurement of hardness and elastic modulus by instrumented indentation: Advances in understanding and refinements to methodology, Journal of Materials Research 19(1) (2004) 3-20
[34] J. Riesch, J. Almanstotter, J.W. Coenen, M. Fuhr, H. Gietl, Y. Han, T. Hoschen, C. Linsmeier, N. Travitzky, P. Zhao, R. Neu, Properties of drawn W wire used as high performance fibre in tungsten fibre-reinforced tungsten composite, IOP Conf. Series: Materials Science and Engineering 139 (2016) 012043.
[35] S. Leber, J. Tavernelli, D.D. White, R.F. Hehemann, Fracture Modes in Tungsten Wire, J Less-Common Met 48(1) (1976) 119-133.
[36] F.J. Humphreys, M. Hatherly, Recrystallization and Related Annealing Phenomena: Second Edition Elsvier (2004) ISBN 78-0-08-044164-1.
[37] O. Engler, V. Randle, Handbook Of Texture Analysis Introduction to Texture Analysis: Macrotexture, Microtexture and Orientation Mapping. Handbook Of Texture Analysis (2010) CRC Press Taylor & Francis Group.
[38] D. Brandon, The Structure of High-Angle Grain Boundaries, Acta Metall. 14 (1966) 1479-1484.
[39] D.A. Hughes, N. Hansen, High angle boundaries formed by grain subdivision mechanisms, Acta Materialia 45(9) (1997) 3871-3886.
[40] G.H. Zahid, Y. Huang, P.B. Prangnell, Microstructure and texture evolution during annealing a cryogenic-SPD processed Al-alloy with a nanoscale lamellar HAGB grain structure, Acta Materialia 57(12) (2009) 3509-3521.
[41] Y. Chen, J.S. Li, B. Tang, H.C. Kou, F.S. Zhang, H. Chang, L. Zhou, Grain boundary character distribution and texture evolution in cold-drawn Ti-45Nb wires, Materials Letters 98 (2013) 254-257.
[42] T. Watanabe, H. Fujii, H. Oikawa, K.I. Arai, Grain-Boundaries in Rapidly Solidified and Annealed Fe-6.5 Mass-Percent Si Polycrystalline Ribbons with High Ductility, Acta Metallurgica 37(3) (1989) 941-952.
[43] V. Randle, Twinning-related grain boundary engineering, Acta Materialia 52(14) (2004) 4067-4081.
[44] J. Qian, C.Y. Wu, J.L. Fan, H.R. Gong, Effect of alloying elements on stacking fault energy and ductility of tungsten, Journal of Alloys and Compounds 737 (2018) 372-376.
[45] X.Z. Xiao, D. Terentyev, A. Ruiz, A. Zinovev, A. Bakaev, E.E. Zhurkin, High temperature nano-indentation of tungsten: modelling and experimental validation, Materials Science & Engineering A accepted for publication (2019) in print.
[46] D.L. Joslin, W.C. Oliver, A New Method for Analyzing Data from Continuous Depth-Sensing Microindentation Tests, J Mater Res 5(1) (1990) 123-126.
[47] W. Oliver, G. Pharr, J Mater Res 19 (2004) 3-20.

Annex I. Size distribution of grains measured by EBSD

ACCEPTED MANUSCRIPT

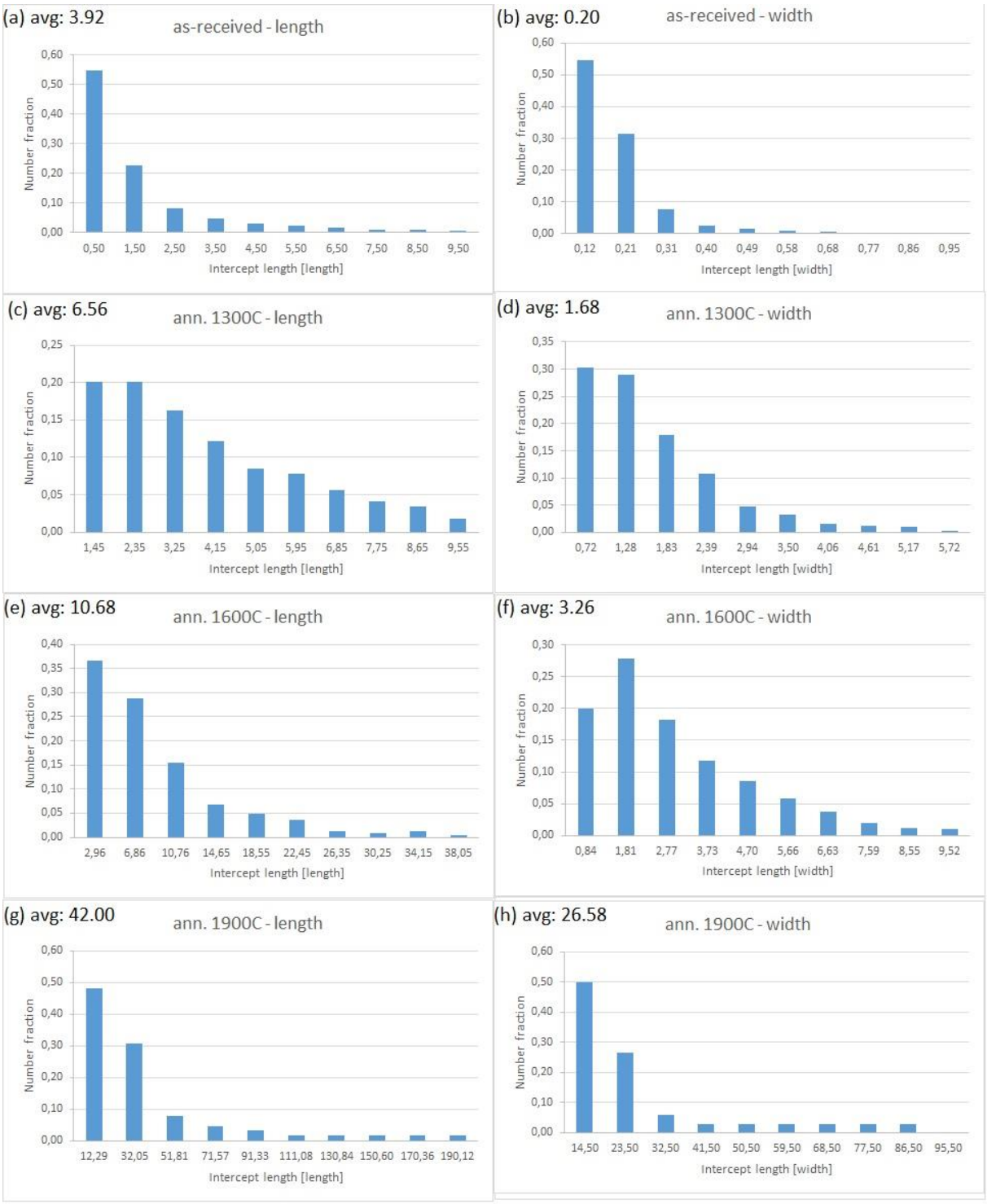

Fig. A1: Length and width distribution of grain boundaries in pure W wire measured in the (a-b) as-received, (c-d) 1300°C, (e-f) 1600°C and (g-h) 1900°C annealed conditions, respectively. At the left upper corner the average values in µm units are displayed.

ACCEPTED MANUSCRIPT

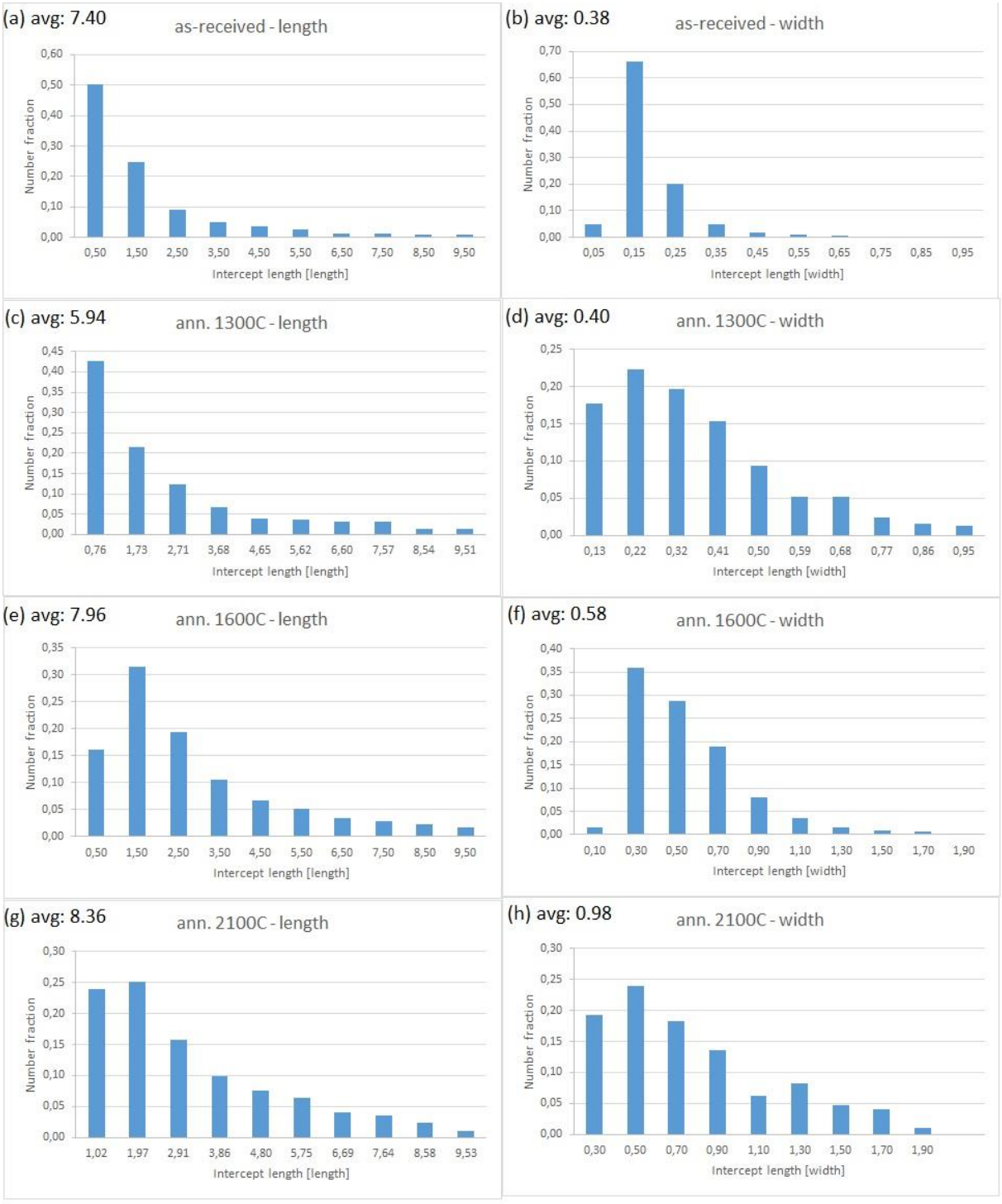

Fig. A2: Length and width distribution of grain boundaries in K-doped wire measured in the (a-b) as-received, (c-d) 1300°C, (e-f) 1600°C and (g-h) 2100°C conditions, respectively. At 2100°C only the small grains were analyzed. At the left upper corner the average values in µm units are displayed.

Annex II. EBSD maps of bulk tungsten in the stress relieved state and annealed states.

ACCEPTED MANUSCRIPT

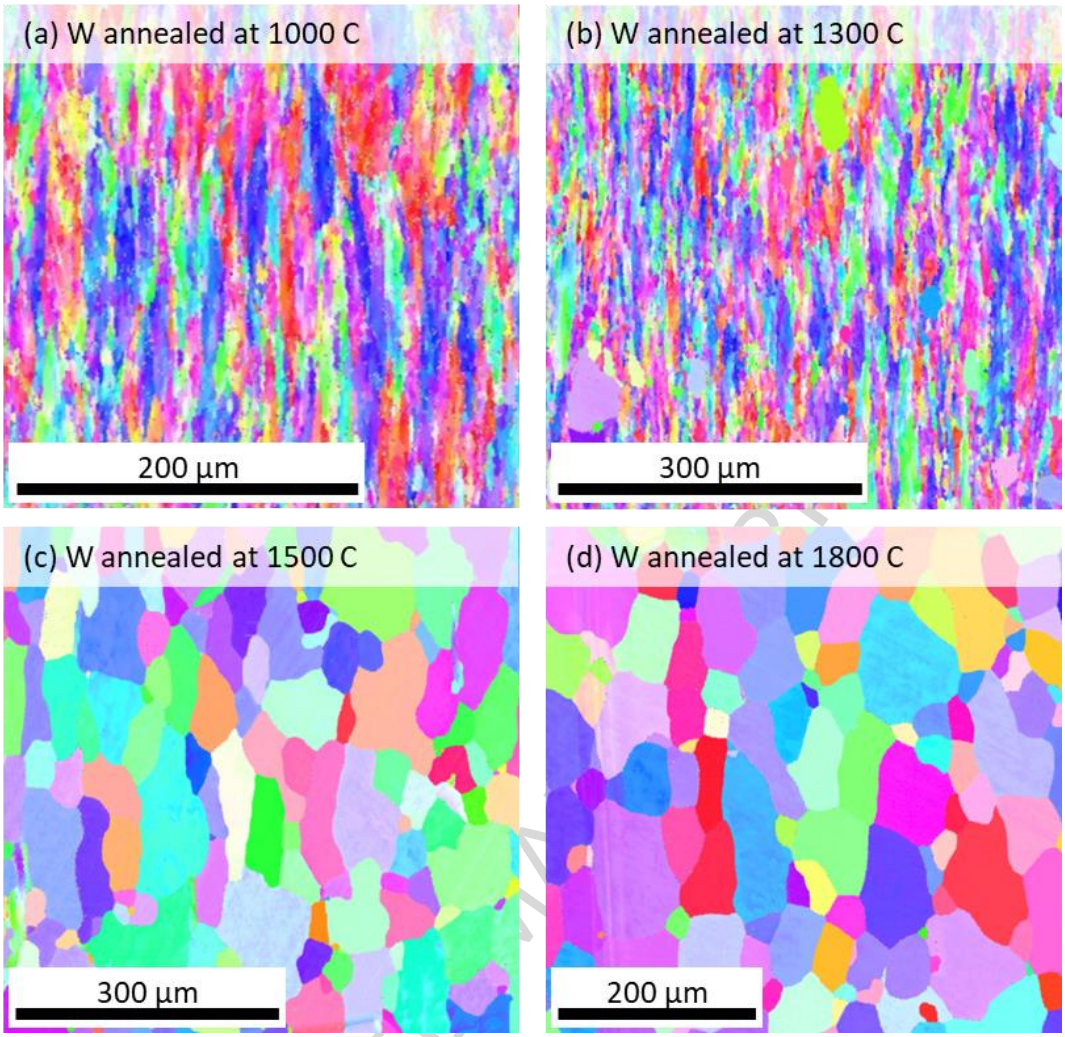

Fig. A3. Microstructure of W in (a) the stress-relieved state and annealed at (b) 1300°C, (c) 1500°C and (d) 1800°C.

Annealing at 1300°C causes nucleation of some new grains but the original texture is still preserved as well as strongly elongated grains are still present. After the annealing at 1500°C, the new grains are formed whose shape is equiaxed and the texture is removed. Almost no difference is revealed between the material annealed at 1500°C and 1800°C. TEM analysis on the samples was performed in [32] and it revealed that such annealing caused the decrease of the dislocation density from 4.5×10^{12} m^{-2} down to 6×10^{11} m^{-2} after annealing at 1300°C, to 3×10^{9} m^{-2} at 1500°C and to 1×10^{8} m^{-2} at 1800°C. The latter value was the limit of the TEM resolution. Small elongated sub-grains were seen to be absent after annealing at 1500°C.

ACCEPTED MANUSCRIPT

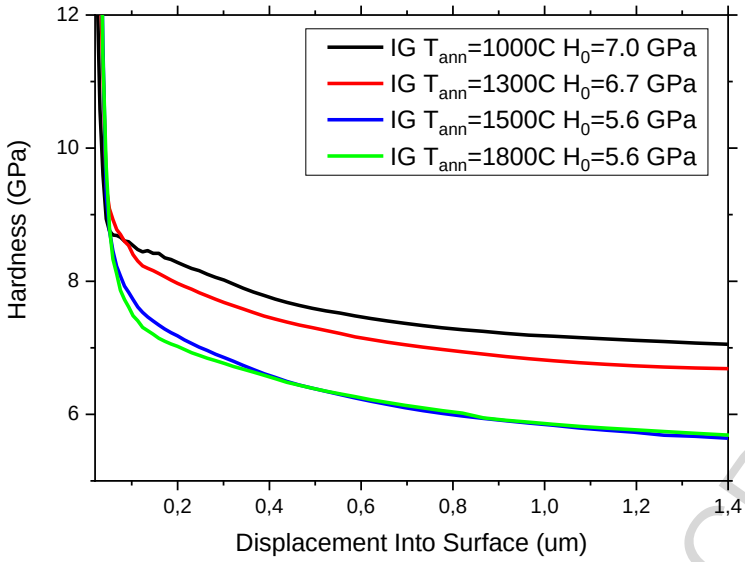

Fig. A4. Hardness-depth curve for the bulk tungsten. Saturated hardness H_0 and annealing temperature (T_{ann} in °C) are shown on the legend.

ACCEPTED MANUSCRIPT

ACCEPTED MANUSCRIPT

Highlights

1. good correlation between nanoindentation hardness and ultimate tensile strength

2. potassium doping suppresses annealing-induced embrittlement at least up to 1900°C

ACCEPTED MANUSCRIPT